NASA TECHNICAL NOTE

NASA TN D-2837

SOME CONSIDERATIONS ON THE USE OF ATMOSPHERIC BRAKING FOR A TRANSFER INTO A MARTIAN ORBIT

by Jacob H. Lichtenstein

Langley Research Center

Langley Station, Hampton, Va.

NATIONAL AERONAUTICS AND SPACE ADMINISTRATION • WASHINGTON, D. C. • JUNE 1965

NASA TN D-2837

SOME CONSIDERATIONS ON THE USE OF ATMOSPHERIC BRAKING FOR A TRANSFER INTO A MARTIAN ORBIT

By Jacob H. Lichtenstein

Langley Research Center
Langley Station, Hampton, Va.

NATIONAL AERONAUTICS AND SPACE ADMINISTRATION

For sale by the Clearinghouse for Federal Scientific and Technical Information
Springfield, Virginia 22151 – Price $2.00

SOME CONSIDERATIONS ON THE USE OF ATMOSPHERIC BRAKING FOR A TRANSFER INTO A MARTIAN ORBIT

By Jacob H. Lichtenstein
Langley Research Center

SUMMARY

26255

An analytical investigation has been made into utilization of the Martian atmosphere for braking in order to transfer from an approach trajectory into an orbit about Mars. The investigation was restricted to that combination of entry angles and velocities that would permit the vehicle to skip out of the atmosphere in order to establish an orbit about the planet, and the vehicle which was used was a blunt-faced body typical of the Apollo spacecraft.

The results show that for a ballistic vehicle the entry corridor is narrow, 3 nautical miles, but with some lift (angle of attack approximately 20°) the corridor widens to about 30 nautical miles. Aerodynamic braking can be utilized to reduce the approach velocity to orbital velocities without exceeding 10 Earth gravitational units and also can be used to change the orbit plane about 10°. In the approach-velocity range of interest, an ablative heat shield for aerodynamic braking was found to require considerably less weight than the rocket fuel for thrust braking.

Author

INTRODUCTION

At the present time, there is intensive interest in both unmanned and manned flights to Mars. This interest is a natural result of the evidence that the conditions on Mars are, at present, considered to be more likely to sustain some form of life than any of the other planets in our solar system and that the planet Mars is one of the easier planets to approach.

A number of studies have been made in the area of manned and unmanned trips to Mars. Some of these studies have been broad mission studies covering flights from Earth to Mars and back again and others have been more detailed studies of certain portions of the overall mission. (See, for instance, refs. 1 to 4.)

In the present paper, only a small portion of the overall mission is considered. Interest is centered on those approaches to Mars which will permit atmospheric braking to be utilized for removal of a considerable amount of excess velocity and thus will aid in establishing an orbit about Mars. Inasmuch as the velocity of approach to Mars will almost assuredly be above the escape velocity for the planet, a very shallow entry into the atmosphere will not

remove sufficient velocity to prevent escape from the planet. On the other hand, an entry that is too steep will result in impact with the surface on the initial entry. This study is concerned principally with the determination of the combinations of entry velocity and angle that define the limits just mentioned. Any circularizing of the orbit will be accomplished by apoapsis-periapsis propulsion after exit from the atmosphere. A sketch depicting these various approach trajectories is shown in figure 1.

For this investigation, the basic vehicle assumed was similar to the Apollo spacecraft, and computations of the trajectory were made for various angles of entry into the atmosphere for several approach velocities from escape velocity upward. Computations were made for a zero-lift condition and also for lift conditions that would result from angles of attack of 4° and 20° with the corresponding lift-drag ratios of 0.08 and 0.4. In addition, some computations were made with other than the ballistic coefficient for the basic configurations by varying the value of drag coefficient to simulate vehicles of different shapes and various amounts of drag augmentation. It is recognized that lift modulation may broaden the entry corridor somewhat; however, lift modulation was not considered in this study. The computations were made on an IBM 7094 electronic data processing system.

SYMBOLS

A	maximum cross-sectional area of heat shield, ft^2
B	corridor width, nautical miles
C_D	drag coefficient
C_X	axial-force coefficient
g_m	acceleration due to gravity at surface of Mars, 13.16 ft/sec^2
h	altitude of vehicle above surface, ft
L/D	lift-drag ratio
Q_c	total convective heat input to vehicle heat shield
Q_R	total radiative heat input to vehicle heat shield
R	radius of heat shield, ft (fig. 2)
R_{hs}	radius of curvature of the face of the heat shield, ft
r	radial distance from center of planet to vehicle, ft
r_m	radius from the center to the surface of Mars, ft

t	time, sec
V	velocity, ft/sec
V_{en}	initial velocity at entry into atmosphere, ft/sec
V_{es}	escape velocity, ft/sec
ΔV_t	total velocity increment necessary to circularize the orbit, ft/sec
W	weight, lb
W/C_DA	ballistic coefficient
α	angle of attack, deg
β	atmospheric density decay factor, per ft
γ	flight-path angle with respect to local horizontal, positive is up, deg
ρ	density of atmosphere, slugs/ft^3
ρ_o	density of atmosphere at surface, slugs/ft^3

METHODS AND COMPUTATIONS

Vehicle and Planetary Characteristics

As mentioned in the introduction, the basic vehicle considered for this investigation was similar to the Apollo spacecraft. A sketch of the spacecraft and pertinent physical characteristics are shown in figure 2. The value of W/C_DA was altered from its basic value of 51.7 by changing the value of C_D. This change simulated vehicles with sharper entry profiles for the lower drag coefficient, and the addition of drag devices for the higher drag coefficients. For the conditions in which lift was utilized for the two high drag coefficients (C_D = 2.00 and 2.50), the normal force was the same as that for the basic condition (that is, C_D = 1.43) at $\alpha = 4^o$ (L/D = 0.08). The combination of the same normal-force coefficient and the additional axial-force coefficient resulted in a smaller effective angle of attack (for C_X = 2.00 and 2.50, $\alpha = 2.6^o$ and 2.0^o, respectively) but in about the same lift-drag ratio (L/D = 0.08 and 0.07, respectively). The values of W/C_DA will be used mainly to identify the vehicle condition for zero angle of attack.

In this investigation, two models of the Martian atmosphere were used. The original model used was one that was representative of information available prior to about the middle of 1963. The second model of the atmosphere, which was based mainly on data supplied to NASA by Dr. Lewis D. Kaplan of the Jet

Propulsion Laboratory, was considerably less dense than the original model. These model atmospheres are shown in figure 3. The formulas for the densities for the two model atmospheres are as follows:

Original model:

$$\rho = \rho_o e^{-K\frac{h}{r_m+h}}$$

$$\rho_o = 3 \times 10^{-5}$$

$$K = 151.64$$

Less-dense model:

$$\rho = \rho_o e^{-\beta h}$$

$$\rho_o = 5.9 \times 10^{-5}$$

$$\beta = 2.96 \times 10^{-5}$$

In both models the value used for the radius of Mars was 11 125 000 feet and for the gravitational constant g_m was 13.16 feet per second^2.

The upper limit of the atmosphere was considered to be 1 140 000 feet. This altitude was selected because the density for the original model of the Martian atmosphere at this altitude was approximately the same as that of the Earth's atmosphere at an altitude of 400 000 feet. This altitude, for most purposes, is considered to be the limit of the sensible atmosphere.

Computations

The trajectories were computed by use of a three-degree-of-freedom system of equations that permitted evaluation of the vertical, longitudinal, and lateral components of the trajectory. The mass of the vehicle was considered centered at the origin of the body axes, and the aerodynamic forces of axial force, normal force, and side force were utilized. The equations used in the computer program are described in the appendix.

For the heat-input computations, the following approximate formulas for the total radiative and convective heat input to the heat shield were inserted in the computation program:

$$Q_R = \int_{t_{entry}}^{t_{exit}} \left\{ \frac{R^2}{2}\left[2 - \left(\frac{R}{R_{hs}}\right)^2\right]\left(0.88 \times 10^6 R_{hs}\right)\rho^{1.25}\left(\frac{V}{10^4}\right)^{7.5} \right\} dt$$

and

$$Q_c = \int_{t_{entry}}^{t_{exit}} \left[\frac{R^{3/2}\left(1.96 \times 10^4\right)}{2} \rho^{1/2} \left(\frac{V}{10^4}\right)^3 \right] dt$$

These relationships were derived by Mr. P. J. Bobbitt of the Langley Research Center and were obtained from a more extensive heat-transfer study. The constants were developed so that the equations would simulate the experimental data presented in reference 5. These equations are applicable for an atmosphere consisting of 20 percent carbon dioxide and 80 percent nitrogen, which is one in which the radiative heating would be high. An atmosphere of this composition is within the range being considered as a possible Martian atmosphere.

The entry velocities considered for this investigation started with the escape velocity of Mars as a minimum and increased, usually, in steps of 10 percent of the average planet velocity around the sun. The ratio of these entry velocities to that for escape velocity is given in the following table:

V_{en}/V_{es}	Velocity, ft/sec	V_{en}/V_{es}	Velocity, ft/sec
1	16 297	3.91	63 754
1.52	24 806	4.40	71 663
1.97	32 116	4.88	79 573
2.46	40 025	5.37	87 482
2.94	47 935	5.85	95 391
3.43	55 844		

Initially, all velocities listed in this table were considered. Since the results of entire mission studies indicated that the most likely approach velocities would be between 20 000 feet per second and 30 000 feet per second, the higher velocities were omitted in some of the later computations.

For each entry velocity considered, trajectories for various entry angles were computed in order to define the width of the entry corridor boundary. The boundaries of this entry corridor are defined by an upper limit (overshoot boundary) where just enough energy is removed to prevent the vehicle from escaping the planet. (For example, the vehicle leaves the atmosphere with parabolic velocity.) The lower limit (undershoot boundary) is that for which enough energy is removed to permit the vehicle to return just to the atmospheric limit. The upper and lower limits of this corridor were defined rather closely, within 0.05°.

In addition to the angular definition of the corridor limits, the width of the corridor in nautical miles was determined. This corridor is considered to be a band measured perpendicular to the flight path. The bottom of the band is

closest to the planet and consequently has the steepest atmospheric entry angle and represents the undershoot boundary. The top of the band is farthest from the planet, and it therefore has the shallowest entry angle and represents the overshoot boundary. The formula for converting the angular corridor limits to the corridor width is given by

$$B = r_a(\cos \gamma_{os} - \cos \gamma_{us})$$

where r_a is the radius to the limit of the atmosphere, and γ_{os} and γ_{us} are the entry angles defining the overshoot and undershoot boundaries, respectively.

The increment in velocity necessary to circularize an orbit after the vehicle had made its initial pass through the atmosphere was determined. The altitude for this orbit was arbitrarily chosen as 188 nautical miles, which was considered the upper limit of the Martian atmosphere. This circularization of the orbit was accomplished in two steps. After exiting from its pass through atmosphere, the vehicle rises to the apoapsis of its orbit, and at this point, enough energy is added to bring the periapsis up to the required altitude (188 nautical miles). When the vehicle subsequently arrives at the periapsis point, enough energy is removed so that its apoapsis altitude is decreased to 188 nautical miles.

RESULTS AND DISCUSSION

The results of this investigation are presented in figures 4 to 19. The entry corridors are given in figures 4 to 7; the velocity decrement and exit velocity, in figures 8 to 11; and the maximum deceleration, in figures 12 and 13. The velocity necessary to circularize the orbit after the spacecraft leaves the atmosphere is shown in figures 14 and 15, and a comparison of the weights necessary for ablative aerodynamic braking and thrust braking is given in figure 16. The plane change capability of the vehicle is shown in figures 17 and 18. The vacuum perigee altitudes for various entry conditions are shown in figure 19.

As a result of some overall Mars mission studies, it has been accepted that the most likely approach velocities to Mars would be about 24 000 feet per second to 26 000 feet per second. Consequently, interest would be centered mainly near these velocities; however, in this study, in order not to limit interest to such a narrow margin, the region of primary concern is assumed to be roughly from 20 000 feet per second to 30 000 feet per second with the respective velocity ratio V_{en}/V_{es} of about 1.3 to 2.0.

Entry Corridor

The boundaries for the entry corridor were defined previously, but briefly they are considered as an upper limit where just enough energy is removed to

prevent the vehicle from escaping the planet and a lower limit where sufficient energy is removed so that the vehicle just escapes the atmosphere after its initial entry.

The angular corridor limits for the various values of W/C_DA are shown in figure 4 for the original atmosphere and in figure 5 for the newer less-dense version. The dashed portion of the curves in figure 4 is merely the extrapolation of the overshoot boundary to the $\gamma = 0^\circ$ point, which would be the overshoot boundary at exactly escape velocity $\left(V_{en}/V_{es} = 1\right)$. The data of figure 4 show that for a zero-lift entry ($\alpha = 0^\circ$), the corridor is very narrow. In the region of primary interest $\left(V_{en}/V_{es}\right.$ between 1.3 and 2.0$\left.\right)$ the corridor is about $1/2^\circ$, and for higher velocities this value gets smaller.

It should be mentioned that when lift was applied to increase the corridor width, positive lift was used for the undershoot boundary so that a steeper entry was allowed, and negative lift was used for the overshoot boundary to permit a shallower entry. The dramatic effect of utilizing lift is clearly seen in figure 4(a). For the basic case of $W/C_DA = 51.7$ with a value of $L/D \approx 0.08$ ($\alpha = 4^\circ$) the corridor widens to about $3/4^\circ$, and for $L/D \approx 0.4$ ($\alpha = 20^\circ$) the corridor becomes larger than 3°. For the lifting conditions the corridor becomes wider with increasing velocity as contrasted to that for the purely ballistic trajectory where the corridor narrows with increasing velocity. The effect on the boundary limits of changing W/C_DA by changing the drag coefficient, at least in the range shown, was small.

The effect of the thinner atmosphere can be seen by comparing figure 5 with figure 4(a). Although the pattern is the same, the magnitude of the corridor is smaller for the thinner atmosphere. In the same region of interest the corridor width for $\alpha = 0^\circ$ is only $1/4^\circ$ instead of $1/2^\circ$ and for $\alpha = 20^\circ$, it is 2° instead of 3°.

These angular corridor widths have been interpreted in terms of nautical miles for the two model atmospheres in figure 6 for the original heavier atmosphere and in figure 7 for the newer thinner atmosphere. The data of figure 6 show that for zero lift, the corridor is quite narrow - only about 4 nautical miles wide for the region of primary interest. With increasing lift, this distance gradually widens to about 47 nautical miles for an $\alpha = 20^\circ$. Similar to its effect on the angular corridor, changing the W/C_DA by changing the drag coefficient had only a small effect on this corridor.

The effect of the thinner atmosphere on the corridor can be seen by comparing figures 7 and 6(a). For the zero lift condition, the corridor was reduced by about 50 percent for the range of the velocity ratios of interest. For the lifting condition, however, the corridor depth was decreased by only about 1/3. However, even for this thinner atmosphere, when lift is utilized the corridor width appears to be within the capability of contemplated guidance systems. The apparent anomaly in which the entry corridor is indicated to be larger for the thinner atmosphere than for the original atmosphere at the velocity ratio of 1 (approximately 85 nautical miles as compared with approximately 65 nautical miles) results from the fact that the initial entry altitude was

arbitrarily maintained at the same value of 1 140 000 feet. Since the undershoot limit is steeper for the thin atmosphere, the corridor therefore appears wider.

Velocity Decrement and Exit Velocity

The velocity decrement that can be achieved by having the vehicle pass through the atmosphere is, of course, dependent upon the depth to which the vehicle penetrates the atmosphere. Therefore, the minimum velocity decrement would occur at the overshoot boundary. These velocity decrements are shown in figures 8 and 9 for the original and the thinner atmosphere, respectively. The data in these figures show that the velocity lost varies linearly with the entrance velocity for both the overshoot and undershoot boundaries and that this line has a slope of 45°. This result indicates a direct variation of velocity lost with entry velocity. This relationship is obvious, of course, for the overshoot boundary because the limiting velocity is constant at the escape velocity (16 297 feet per second). However, since the velocity lost for the undershoot boundary also is almost a linear variation with about the same slope, it suggests that the limiting exit velocity is about the same for all these entry velocities, also.

The velocity of the vehicle as it leaves the atmosphere is shown plotted against entry velocity in figures 10 and 11 for the original and newer atmospheres, respectively. It can be seen that these exit velocities are, indeed, about the same for all the entry velocities and the magnitude is slightly below orbital velocity for a low-altitude orbit (188 nautical miles). Examination of these figures shows that for the original atmosphere there is no perceptible trend of exit velocity with entry velocity for the $\alpha = 0^{\circ}$ condition. For the $\alpha = 20^{\circ}$ condition the trend is for exit velocity to decrease with an increase in entry velocity. As a consequence, for the velocity region of primary interest, the lifting condition seems to be able to develop an appreciably greater velocity decrement than the nonlifting condition.

For the newer atmosphere (fig. 11) the trends in the variation of exit velocity with entry velocity are just about the same as for the original atmosphere; however, the values are higher by about 500 feet per second.

Maximum Deceleration

The maximum deceleration that the vehicle will experience during the portion of its flight within the atmosphere is important for both manned and unmanned vehicles. For the unmanned vehicle this acceleration information is important for structural and payload considerations. The manned version has an additional restriction that the man can withstand an acceleration of only 10 to 12 Earth g and this for only a short period of time. After a lengthy trip to Mars in which the crew may have been in a zero or near zero gravity environment, their ability to withstand high forces may be considerably diminished. The data showing the maximum decelerations are shown in figures 12 and 13 for the original and thinner versions of the Martian atmosphere.

The data of figure 12 for the original atmosphere indicate that, for the approach velocities below about 40 000 feet per second and zero lift, the deceleration does not exceed 10 Earth g. When lift is utilized, the deceleration is somewhat higher at the lower limit of the approach corridor. This difference is probably due to the fact that utilizing lift permits a steeper angle of entry. However, utilization of the full lift to permit steeper entries in order to widen the entry corridor would result in higher g loads than desirable. Therefore, the undershoot boundary may well be defined by the g load limit. Changing W/C_DA by changing the drag coefficient by the amounts in this investigation did not seriously affect the previous results.

For the less-dense atmosphere the maximum decelerations were somewhat higher than for the original atmosphere because of the larger atmospheric density decay factor. In the thinner atmosphere with zero lift a deceleration of 10 Earth g occurs for an entry velocity of only about 35 000 feet per second. The data in figure 13 show that the application of lift to permit a steeper approach angle at about this velocity results in excessively high decelerations. As a matter of fact, a value of 10 Earth g is exceeded at 26 000 feet per second. As a consequence, full utilization of lift to permit widening the approach corridor will not be available. Therefore, modulation of the lift will be necessary to maintain maximum corridor width without exceeding permissible deceleration limits.

Velocity Necessary to Circularize Orbits

Since one of the purposes of the present work was to establish an orbit around Mars it is necessary to determine what has to be done in order to accomplish this result. The approach velocity will exceed the orbital velocity; therefore some braking to reduce the velocity will be required. A study of all the computations that were made showed that only for the lowest velocity considered (16 297 feet per second) and at entry angles that were considerably shallower than that for the undershoot boundary was more than one orbit about the planet possible. For all other conditions, the second entry resulted in an impact. Consequently, if a permanent orbit is to be established it must be done during this first skipout. The procedure followed for circularizing the orbit was previously described in the section "Computations." The total velocity necessary to establish the orbit after braking is shown in figures 14 and 15 for the original and newer atmospheric models, respectively.

The data in figure 14 for the basic W/C_DA show that the undershoot boundary, with or without lift, requires a considerably lower amount of velocity to be added than does the overshoot boundary. This results from the fact that the overshoot-boundary exit velocities are considerably higher, about 4800 feet per second higher, and this difference accounts for most of the extra velocity required. Actually, the data for the overshoot boundary are for the points that fell just inside the boundary. The scatter of the data, particularly for the overshoot boundary, results from the lack of exactness in the entry angle used as the boundary value because an exact determination of this angle would have required a tremendous number of computations. As it is, the boundary value was generally found to be within 0.05°, and further refinement did not at first appear warranted. However, because the scatter was so great, some additional

computations were made for the undershoot boundary in which the boundary was refined to within 0.01°. Originally, the scatter for the undershoot boundary was as much as that for the overshoot boundary, but the tighter definition of the boundary resulted in a vast improvement in the undershoot data. The variation of ΔV_t with entry velocity for the undershoot boundary is directly related to the velocity at exit from the atmosphere. (See fig. 10.) The results for the other values of W/C_DA are essentially the same as for the basic condition and therefore are not presented.

The data for the velocity to be added for the newer thinner atmosphere are shown in figure 15, and the results are very similar to those for the original atmosphere in both magnitude and trends.

The data shown are for establishment of an orbit at an altitude of 188 nautical miles, which was arbitrarily chosen for both atmospheres. For somewhat higher orbital altitudes (for instance, 400 and 500 nautical miles as proposed in some studies) which can be achieved by using an entry angle somewhat above the undershoot boundary value, the velocity increment will be slightly lower because of the variation of orbital velocity with altitude.

Comparison of Heat Shield and Thrust Fuel Weight

Because the vehicle will approach Mars with a velocity higher than the velocity of escape from the planet, braking of some sort will be necessary in order to establish an orbit about the planet. It is interesting to compare the weights required for braking by aerodynamic means and for braking by the application of thrust. (See fig. 16.)

In order to assess the weight of the heat shield some approximate computations of the total heat input were made for the Apollo spacecraft for angles of attack of 0° and 20° and for entry velocities up to 32 116 feet per second. Computations were made for the less-dense atmosphere and for the undershoot boundary points because this represented the condition in which the maximum amount of heat would be absorbed. The data shown in figure 16 for the two angles of attack represent the weights resulting from the different heat inputs that arose from the two different entry trajectories. The thrusting weights shown are those required to achieve the same velocity decrement as was obtained by aerodynamic braking.

A representative figure of 5000 Btu per pound was used for the heat absorption capability of the heat shield. However, the weight was arbitrarily increased by 50 percent to allow for structural considerations and for some insulation. For computation of the fuel weight required, specific impulses of 300 seconds and 900 seconds were used as representative of typical storable fuels and nuclear fuels, respectively. For none of these computations was account taken of the necessary engine or shielding weights. The fuel weights for $\alpha = 0°$, and $\alpha = 20°$ is only the weight required to achieve the same velocity decrement as that which was attained aerodynamically at these angles of attack.

The data in figure 16 show the decided advantage in weight obtained by the heat shield and aerodynamic braking over the use of thrust for braking. Also shown is the relatively rapid rise in heat-shield weight with increasing velocity. This can be seen by comparing the relative weights at 24 400 feet per second and 32 100 feet per second. At an entry velocity of 24 400 feet per second the storable fuel weight required is about 14 times as much as the heat-shield weight but at 32 100 feet per second it is only about 4 times as much. At velocities only slightly higher than this, the advantage probably reverses for this vehicle. The effect of a 20° angle of attack is to increase the necessary weight slightly for both the heat shield and fuel required. This difference results from the fact that with the lifting body, a steeper entry angle is possible with a consequent deeper penetration of the atmosphere. This penetration, in turn, results in a greater heat transfer to the vehicle so that the heavier heat shield is required and also in a greater velocity decrement that requires the additional fuel.

Plane-Change Capability

It is recognized that when a spacecraft arrives at Mars its trajectory may not be in the plane desired for the orbit to be established. Therefore, an attempt was made to assess the ability of the vehicle to utilize the atmosphere to alter its orbit plane as well as to provide braking. Since it is of interest to evaluate the maximum amount of plane-change capability, the computations were made for the steepest entry angle into the atmosphere that would just permit the vehicle to escape again from the atmosphere for a no-lift condition, but with either 10° or 20° of sideslip. This is comparable to the concept of a trim angle of attack of 10° or 20° combined with a roll angle of 90° so that the lift vector is oriented to the side.

The data from these computations are shown in figure 17 for the original atmosphere model and in figure 18 for the newer atmosphere model. The data for both atmospheres are similar in nature in that the magnitude of the plane change generally varies linearly with both angle of sideslip and initial entry velocity. The ability of a vehicle to change its orbit plane is considerably less for the thin atmosphere model than for the original model. For the entry velocities of primary interest (up to about 32 000 feet per second) and sideslip angles of 20°, this reduction is about 30 percent. However, even for this thin atmosphere a plane change of 8° to 10° can be achieved.

Vacuum Periapsis

It is realized that the vacuum periapsis altitude is often considered an important parameter of an approach trajectory. Although this parameter was not utilized in this paper, the values were computed and these data are shown in figure 19 so that the vacuum periapsis altitude for any combination of entry velocity and angle can readily be obtained.

CONCLUDING REMARKS

An analytical investigation has been made into utilization of the Martian atmosphere for braking in order to transfer from an approach trajectory into an orbit about Mars. The investigation was restricted to that combination of entry angles and velocities that would permit the vehicle to skip out of the atmosphere in order to establish an orbit about the planet, and the vehicle which was used was a blunt-faced body typical of the Apollo shape.

The results of the investigation show that the entry corridor for establishing these orbits at zero angle of attack is quite narrow, on the order of $1/4^\circ$ or 3 nautical miles for zero lift. For lift corresponding to an angle of attack of 20° (lift-drag ratio approximately 0.4) this corridor widens to 2° or 30 nautical miles. By the use of aerodynamic braking the velocity can be reduced from above escape velocity down to about orbital velocity, and for approach velocities of primary interest (20 000 feet per second to 30 000 feet per second) this reduction can be accomplished without exceeding 10 Earth g. However, the utilization of lift to broaden the entry corridor by permitting steeper entries may result in excessively high deceleration loads. Consequently, the undershoot boundary may be defined by the permissible deceleration loading and, therefore, a scheme for modulating the lift would be necessary. Although not specifically investigated in this paper, the results indicated that the use of lift would make it possible to select a desired final orbit altitude from a wider set of initial conditions.

The weight of the heat shield necessary to absorb the energy that must be dissipated during atmospheric braking was found to be considerably less than the weight of rocket fuel necessary to accomplish the same reduction in velocity. The rocket fuel was from 4 to 14 times as heavy as the heat shield depending upon the entry velocity. The atmosphere can be used not only for braking but also for changing the plane of the orbit. For the conditions considered in this investigation a change in the orbit plane of 8° to 10° can be achieved.

Langley Research Center,
National Aeronautics and Space Administration,
Langley Station, Hampton, Va., January 26, 1965.

APPENDIX

EQUATIONS OF MOTION

A three-degree-of-freedom system of equations of motion were used for the computations. These equations were written with respect to an inertial-axis system fixed at the center of the spherical, nonrotating planet. The positive X inertial axis passed outward through the initial location of the vehicle as it approached the planet. The three force equations may be represented in matrix form as follows:

$$\begin{bmatrix} \ddot{x} \\ \ddot{y} \\ \ddot{z} \end{bmatrix} = \frac{1}{m} \begin{bmatrix} \quad \\ T_{B \text{ to } I} \\ \quad \end{bmatrix} \begin{bmatrix} F_X \\ F_Y \\ F_Z \end{bmatrix} + \begin{bmatrix} \quad \\ T_{G \text{ to } I} \\ \quad \end{bmatrix} \begin{bmatrix} 0 \\ 0 \\ g_{Z,G} \end{bmatrix}$$

The three axes systems used are shown in sketches A1 and A2.

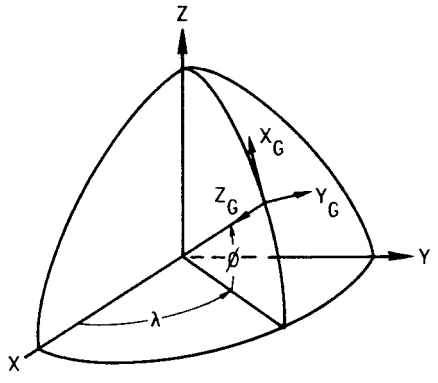

Sketch A1

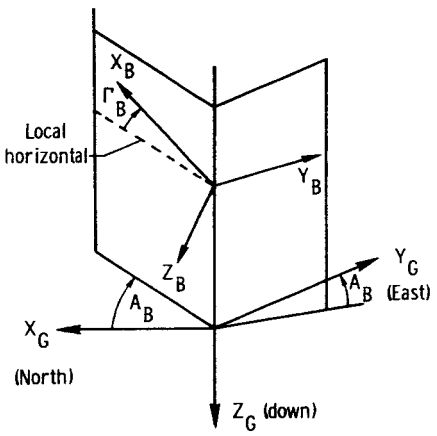

Sketch A2

Symbols are defined as follows:

X,Y,Z	inertial axes system with the origin at center of planet
x,y,z	distances along inertial axes
X_G,Y_G,Z_G	planetocentric axes system with the origin on the surface and oriented as shown
X_B,Y_B,Z_B	body-axis system with origin at center of gravity of vehicle with the X_B axis oriented forward and the Y_B axis to the side

APPENDIX

λ	longitude angle
ϕ	latitude angle
A_B	azimuth angle of vehicle body axes
Γ_B	pitch angle of vehicle body axes
F_X, F_Y, F_Z	aerodynamic forces along the vehicle body axes
A_I	azimuth angle of flight path
Γ_I	inclination of flight path
$g_{Z,G}$	gravity compound along the planetocentric axes, same as g_m
m	mass of vehicle, slugs
$T_{B \text{ to } I}$	conversion matrix from body axes to inertial axes
$T_{G \text{ to } I}$	conversion matrix from planetocentric axes to inertial axes

A dot over a symbol means differentiation with respect to time. From sketch A1, the conversion matrix from the planetocentric axes to inertial axes is seen to have the following form:

$$T_{G \text{ to } I} = \begin{bmatrix} -\sin\phi\cos\lambda & -\sin\lambda & -\cos\phi\cos\lambda \\ -\sin\phi\sin\lambda & \cos\lambda & -\cos\phi\sin\lambda \\ \cos\phi & 0 & -\sin\phi \end{bmatrix}$$

From sketch A2, the conversion matrix from the body axes to planetocentric axes is seen to have the following form:

$$T_{B \text{ to } G} = \begin{bmatrix} \cos\Gamma\cos A_B & -\sin A_B & \sin\Gamma\cos A_B \\ \cos\Gamma\sin A_B & \cos A_B & \sin\Gamma\sin A_B \\ -\sin\Gamma & 0 & \cos\Gamma \end{bmatrix}$$

The absence of a roll angle in this matrix is discussed subsequently. The body aerodynamic forces were obtained from the expressions:

APPENDIX

$$F_X = qAC_X$$

$$F_Y = qAC_Y$$

$$F_Z = qAC_Z$$

where

A	reference area
q	dynamic pressure, $\frac{1}{2}\rho V^2$
C_X, C_Y, C_Z	aerodynamic coefficients along the X-, Y-, and Z-axes, respectively

Inasmuch as the angle of attack or sideslip was held constant throughout a run, the proper values of the aerodynamic coefficients for that angle of attack or sideslip were used.

For a symmetric vehicle such as used herein the lift produced is proportional to the total angle of attack. In these computations the lift was either in the vertical plane (in which case C_Z was used with $C_Y = 0$) or in the horizontal plane (in which case C_Y was used and $C_Z = 0$). This situation would be similar to one in which a normal-force type of coefficient was used and the roll angle was considered to be either 0° or 90°.

For these computations, the roll angle with respect to the local horizontal was always considered zero and therefore the conversion matrix from the body axes to inertial axes has the form:

$$T_{B \text{ to } I} = T_{G \text{ to } I} T_{B \text{ to } G}$$

When these two matrices are multiplied, the expanded matrix becomes:

$$T_{B \text{ to } I} = \begin{bmatrix} (-\sin\phi\cos\lambda\cos\Gamma_I\cos A_B & -\sin\lambda\cos\Gamma_I\sin A_B & +\cos\phi\cos\lambda\sin\Gamma_I) \\ (-\sin\phi\sin\lambda\cos\Gamma_I\cos A_B & +\cos\lambda\cos\Gamma_I\sin A_B & +\cos\phi\sin\lambda\sin\Gamma_I) \\ (\cos\phi\cos\Gamma_I\cos A_B & + 0 & +\sin\phi\sin\Gamma_I) \end{bmatrix}$$

$$\begin{pmatrix} \sin\phi\cos\lambda\sin A_B & - \sin\lambda\cos A_B & + 0 \\ \sin\phi\sin\lambda\sin A_B & + \cos\lambda\cos A_B & + 0 \\ -\cos\phi\sin A_B & + 0 & + 0 \end{pmatrix}$$

$$\begin{bmatrix} (-\sin\phi\cos\lambda\sin\Gamma_I\cos A_B & -\sin\lambda\sin\Gamma_I\sin A_B & -\cos\phi\cos\lambda\cos\Gamma_I) \\ (-\sin\phi\sin\lambda\sin\Gamma_I\cos A_B & +\cos\lambda\sin\Gamma_I\sin A_B & -\cos\phi\sin\lambda\cos\Gamma_I) \\ (\cos\phi\sin\Gamma_I\cos A_B & + 0 & -\sin\phi\cos\Gamma_I) \end{bmatrix}$$

APPENDIX

The inertial velocities were obtained by integrating the force equations

$$\dot{x} = \int \ddot{x}\, dt + \dot{x}_o$$

$$\dot{y} = \int \ddot{y}\, dt + \dot{y}_o$$

$$\dot{z} = \int \ddot{z}\, dt + \dot{z}_o$$

where $\dot{x}_o, \dot{y}_o, \dot{z}_o$ are initial conditions depending upon the initial entry velocity and flight-path angle. The total inertial velocity was obtained from:

$$V = \sqrt{\dot{x}^2 + \dot{y}^2 + \dot{z}^2}$$

The displacements along the inertial axes were obtained by integrating the velocity equations:

$$x = \int \dot{x}\, dt + x_o$$

$$y = \int \dot{y}\, dt + y_o$$

$$z = \int \dot{z}\, dt + z_o$$

Here again x_o, y_o, z_o are initial conditions. The inertial axes were alined so that the X-axis passed through the initial entry point and the initial entry velocity vector was in the X-Z plane. Therefore, y_o and $z_o = 0$ and $x_o = r_m + h_o$. The altitude was obtained from

$$h = x - r_m$$

For entries with no sidewise disturbance the orbits remain in the x-z plane and therefore pass over the Z-axis. Consequently, the maximum latitude would always be 90^o, and any change in plane would result in a condition where the maximum latitude for the orbit would no longer be 90^o. The plane-change angle, ψ, was obtained from the expression:

$$\psi = 90^o - \phi_{max}$$

REFERENCES

1. Chapman, Dean R.: An Approximate Analytical Method for Studying Entry Into Planetary Atmospheres. NASA TR R-11, 1959. (Supersedes NACA TN 4276, 1958.)

2. Chapman, Dean R.: An Analysis of the Corridor and Guidance Requirements for Supercircular Entry Into Planetary Atmospheres. NASA TR R-55, 1960.

3. Pritchard, E. Brian: Survey of Velocity Requirements and Reentry Flight Mechanics for Manned Mars Missions. Preprint No. 64-13, Am. Inst. Aeron. Astronaut., Jan. 1964.

4. Napolin, A. L.; and Mendez, J. C.: Target Orbit Selection for Mars Missions Using Aerodynamic Maneuvering. Preprint No. 64-14, Am. Inst. Aeron. Astronaut., Jan. 1964.

5. James, Carlton S.: Experimental Study of Radiative Transport From Hot Gases Simulating in Composition the Atmosphere of Mars and Venus. AIAA J., vol. 2, no. 3, Mar. 1964, pp. 470-475. (Available also as NASA RP-174.)

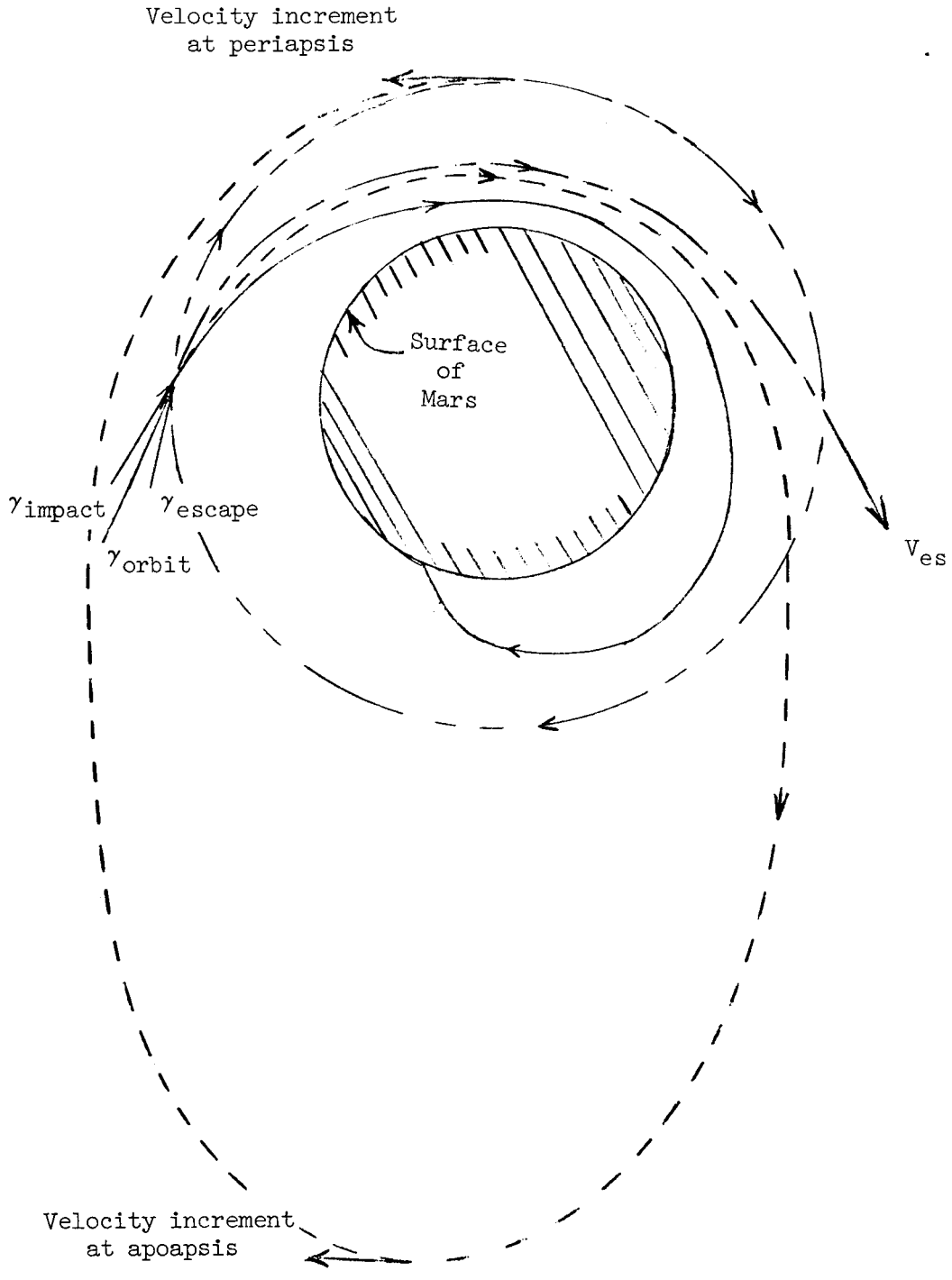

Figure 1.- Typical trajectories depicting a first-pass impact, an orbit, and an escape situation for a Martian atmospheric approach. In addition, the location and direction of the incremental velocities necessary to circularize the orbit are shown.

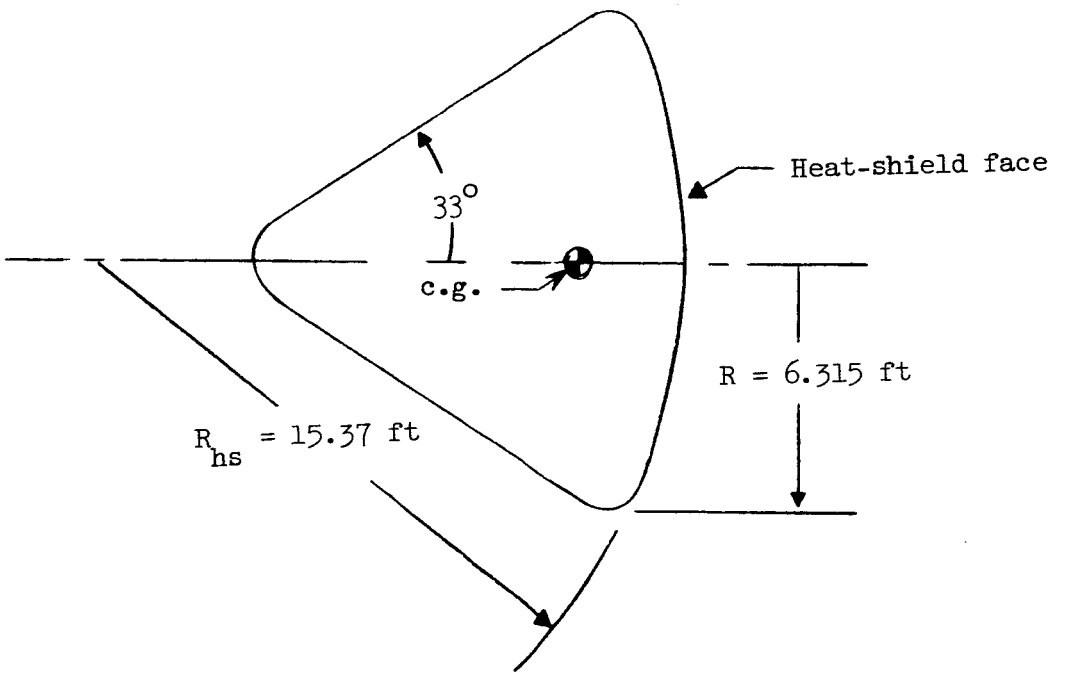

Cross-section area A	129.26 sq ft
Weight of vehicle	9561 lb

C_D	$\frac{W}{C_D A}$ $\frac{lb}{sq\ ft}$
1.00	74.0
1.43	51.7 (basic condition)
2.00	37.0
2.50	29.6

Figure 2.- Sketch and pertinent data for the vehicle used in this investigation.

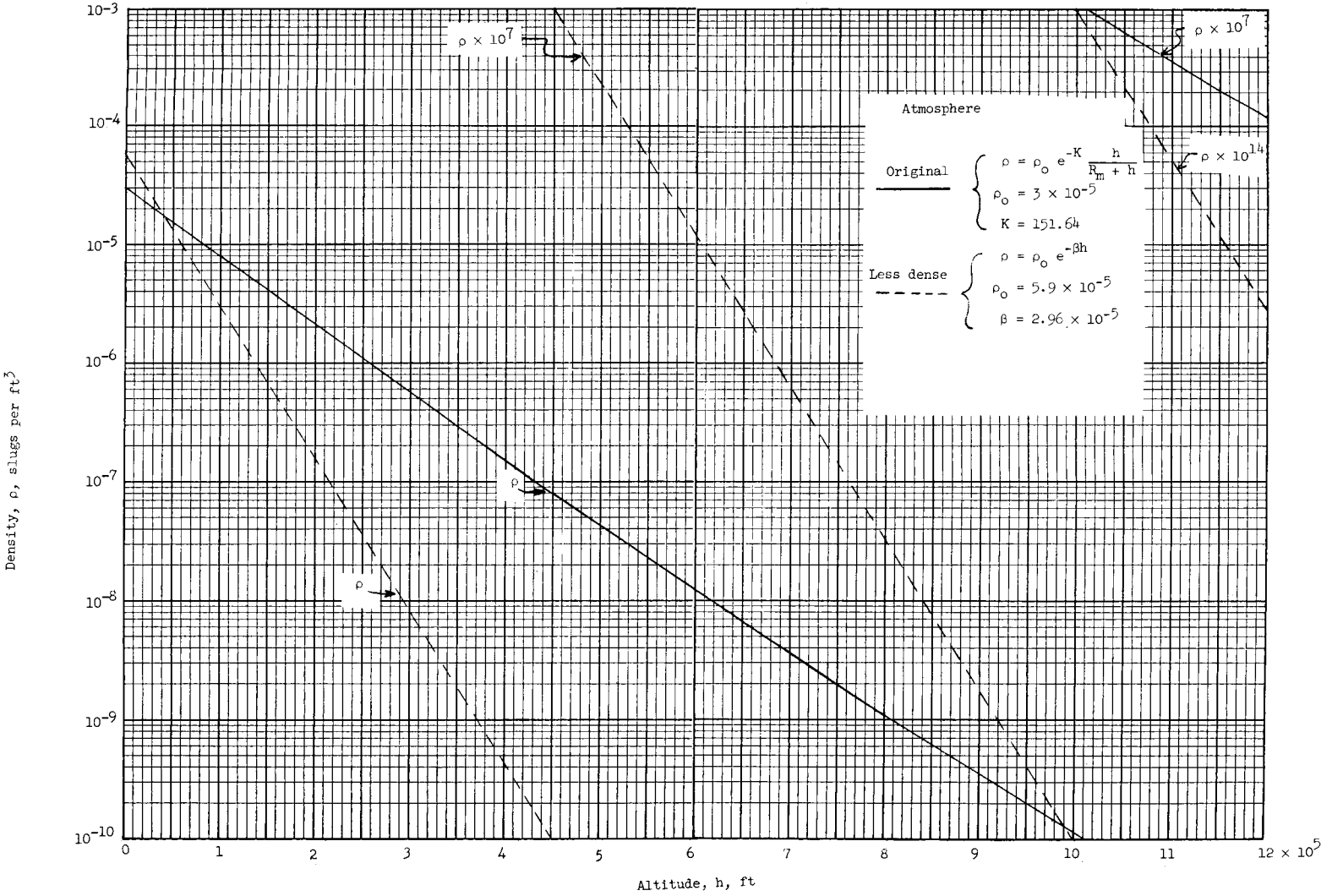

Figure 3.- Models of both the original and newer less-dense version of the Martian atmosphere used in the computations.

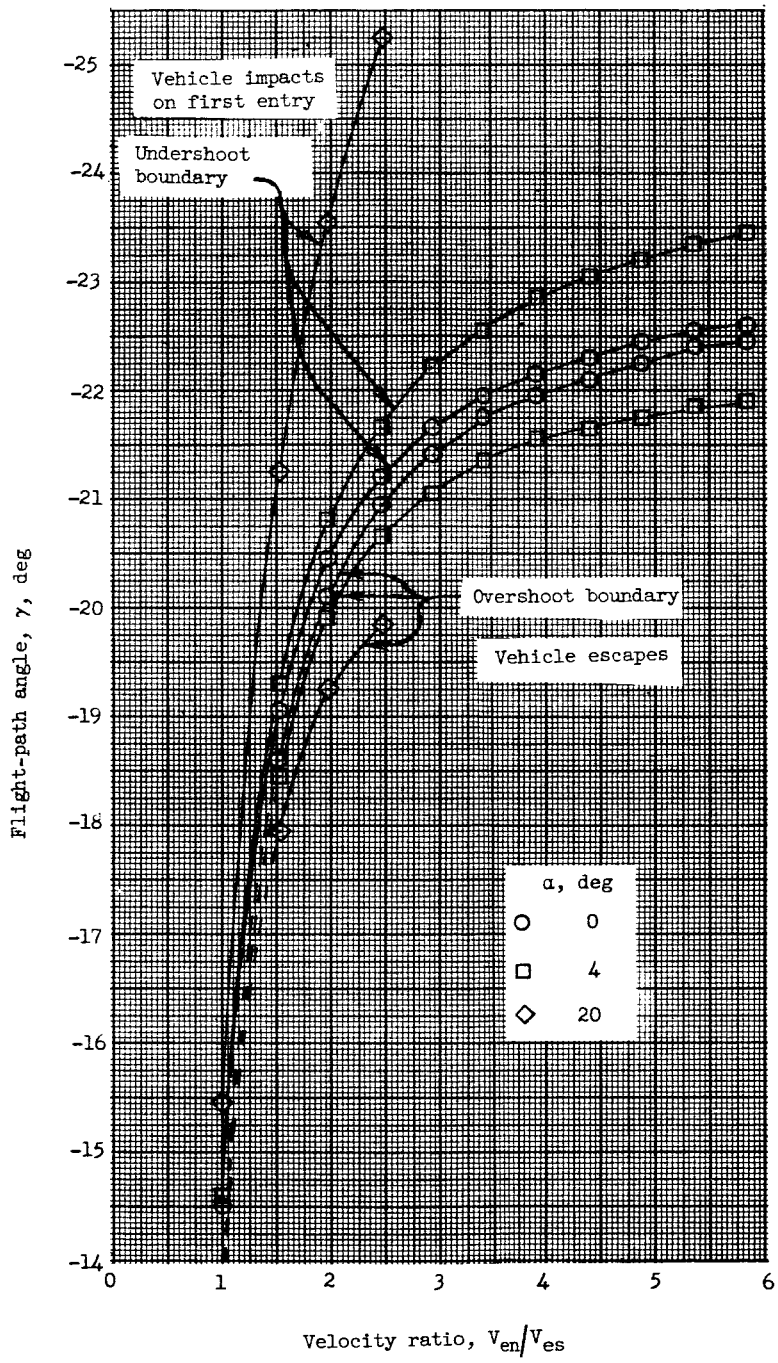

(a) Basic condition; $\frac{W}{C_D A}$ = 51.7 lb/ft^2; C_D = 1.43.

Figure 4.- Angular entry corridor plotted against entry velocity ratio for the original atmosphere model.

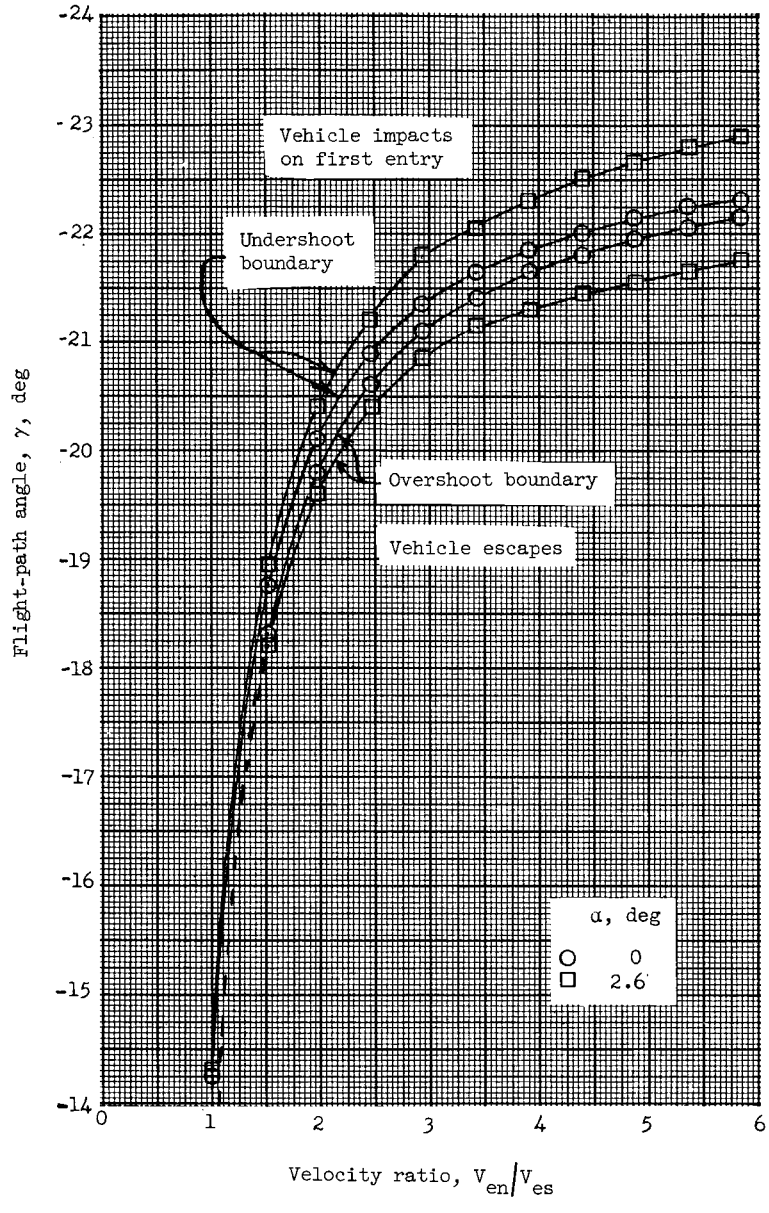

(b) $\frac{W}{C_D A}$ = 37.0 lb/ft^2; C_D = 2.00.

Figure 4.- Continued.

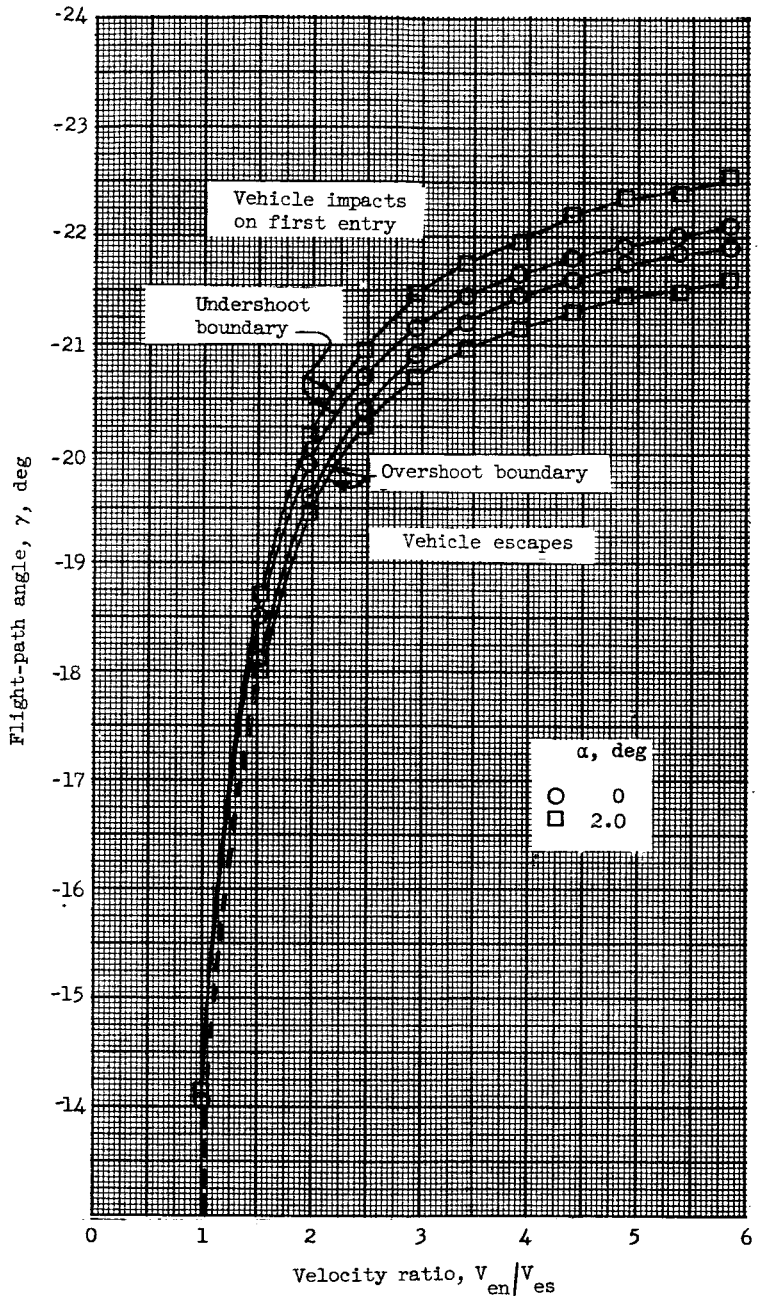

(c) $\frac{W}{C_D A}$ = 29.6 lb/ft^2; C_D = 2.50.

Figure 4.- Continued.

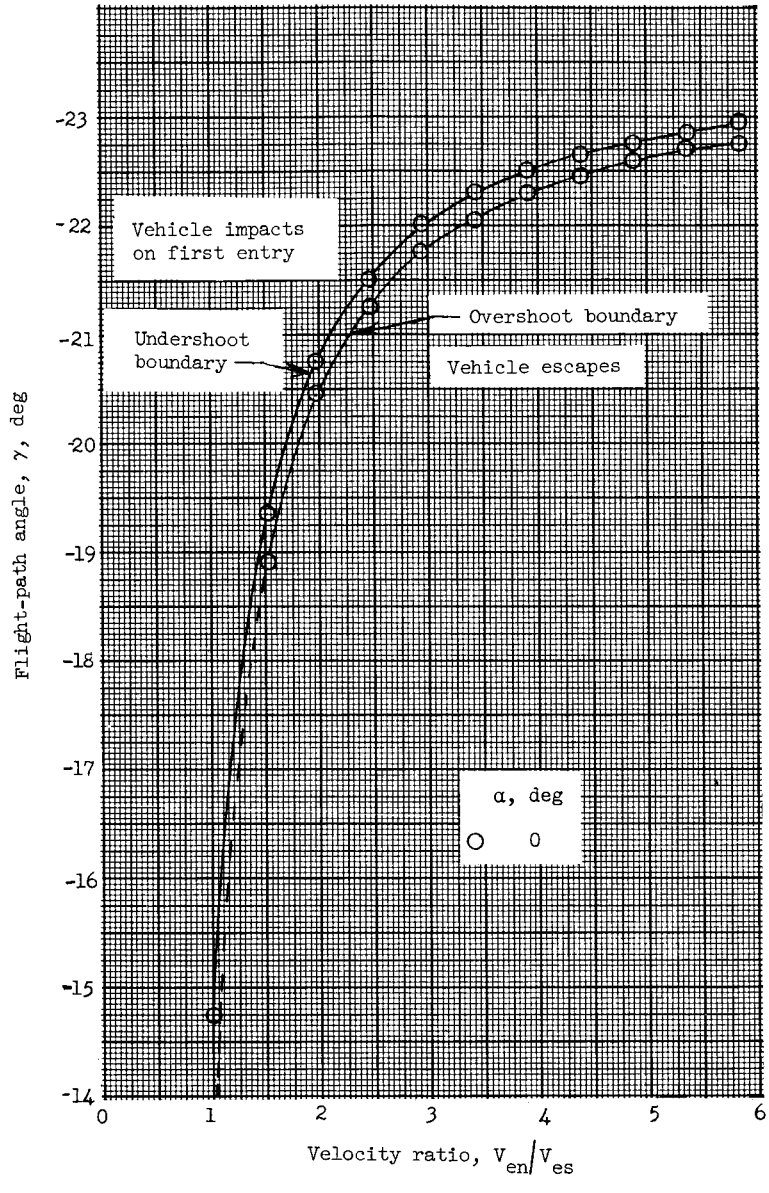

(d) $\frac{W}{C_D A}$ = 74.0 lb/ft^2; C_D = 1.00.

Figure 4.- Concluded.

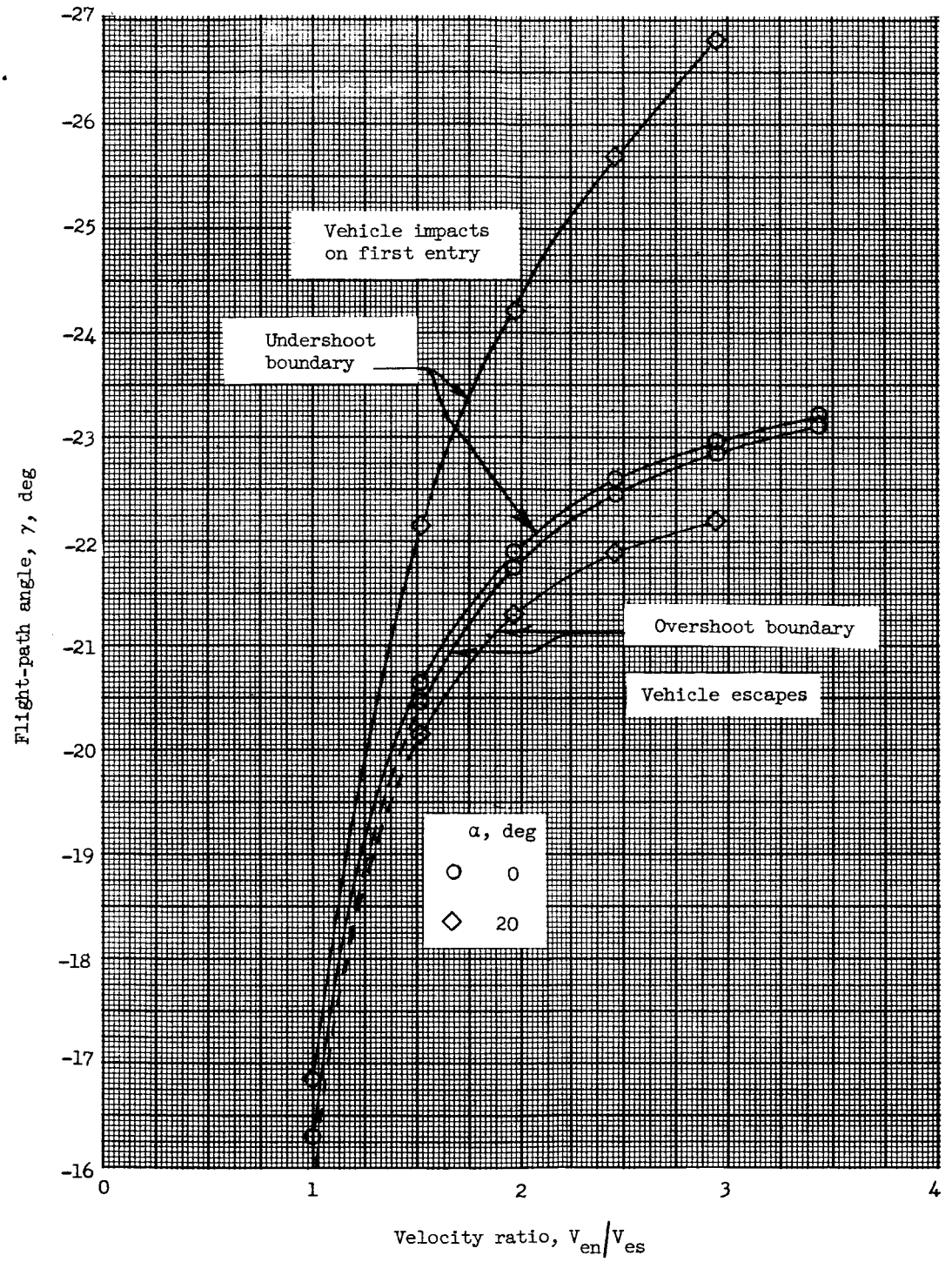

Figure 5.- Angular entry corridor plotted against entry velocity ratio for the newer atmosphere model. Basic condition; $\frac{W}{C_D A}$ = 51.7 lb/ft^2; C_D = 1.43.

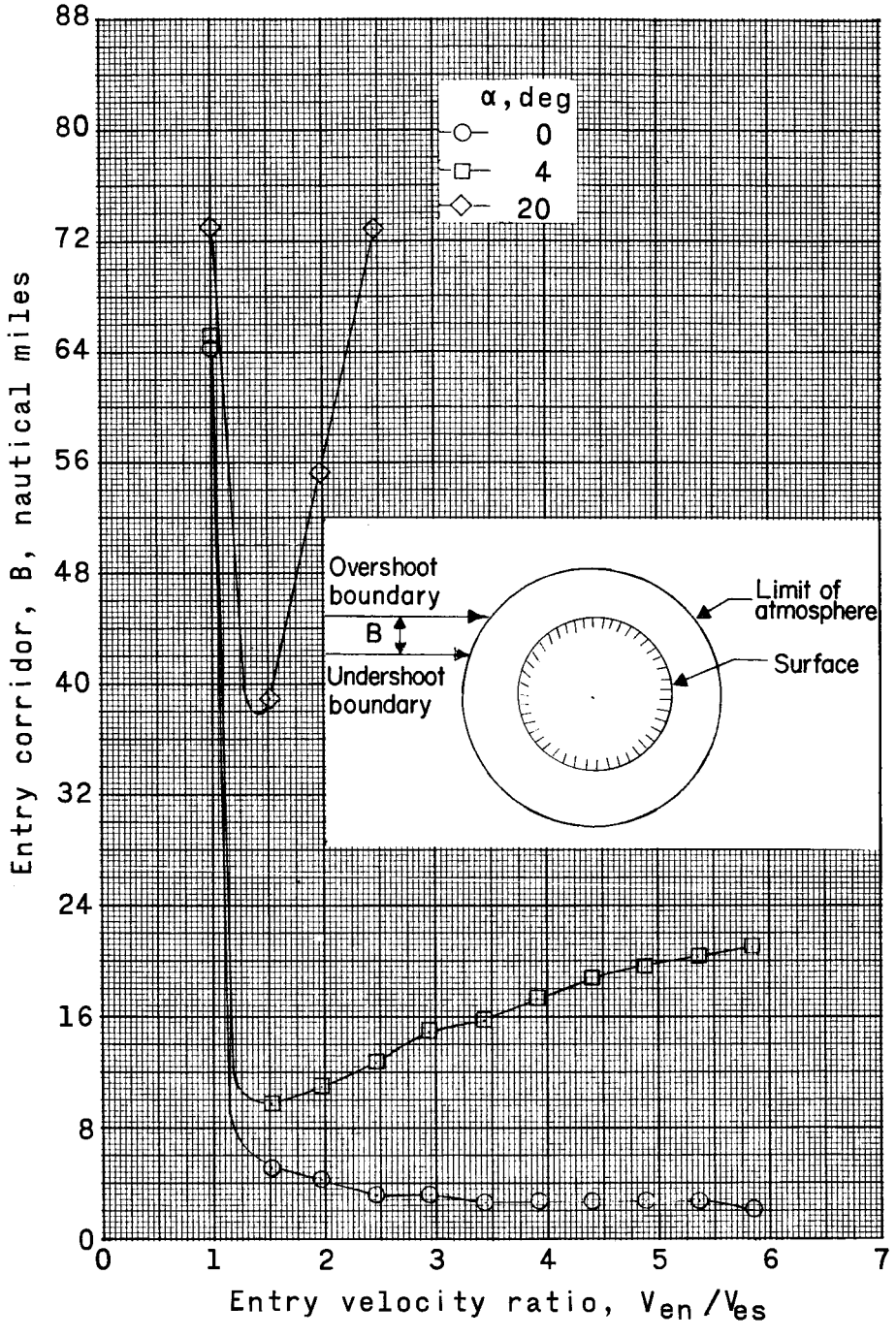

(a) Basic condition; $\frac{W}{C_D A}$ = 51.7 lb/ft^2; C_D = 1.43.

Figure 6.- Entry corridor in nautical miles plotted against entry velocity ratio for original atmosphere.

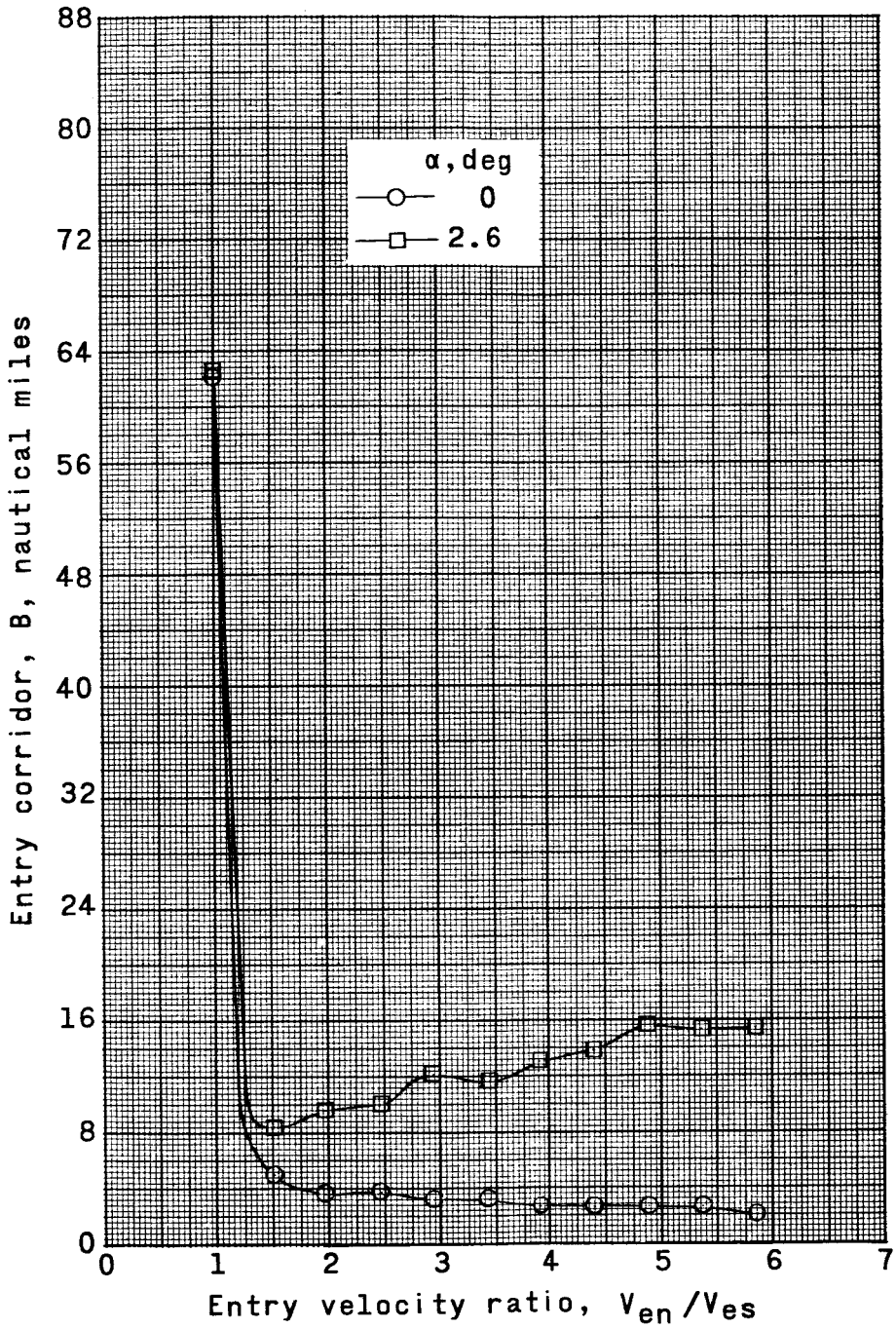

(b) $\frac{W}{C_D A}$ = 37.0 lb/ft^2; C_D = 2.00.

Figure 6.- Continued.

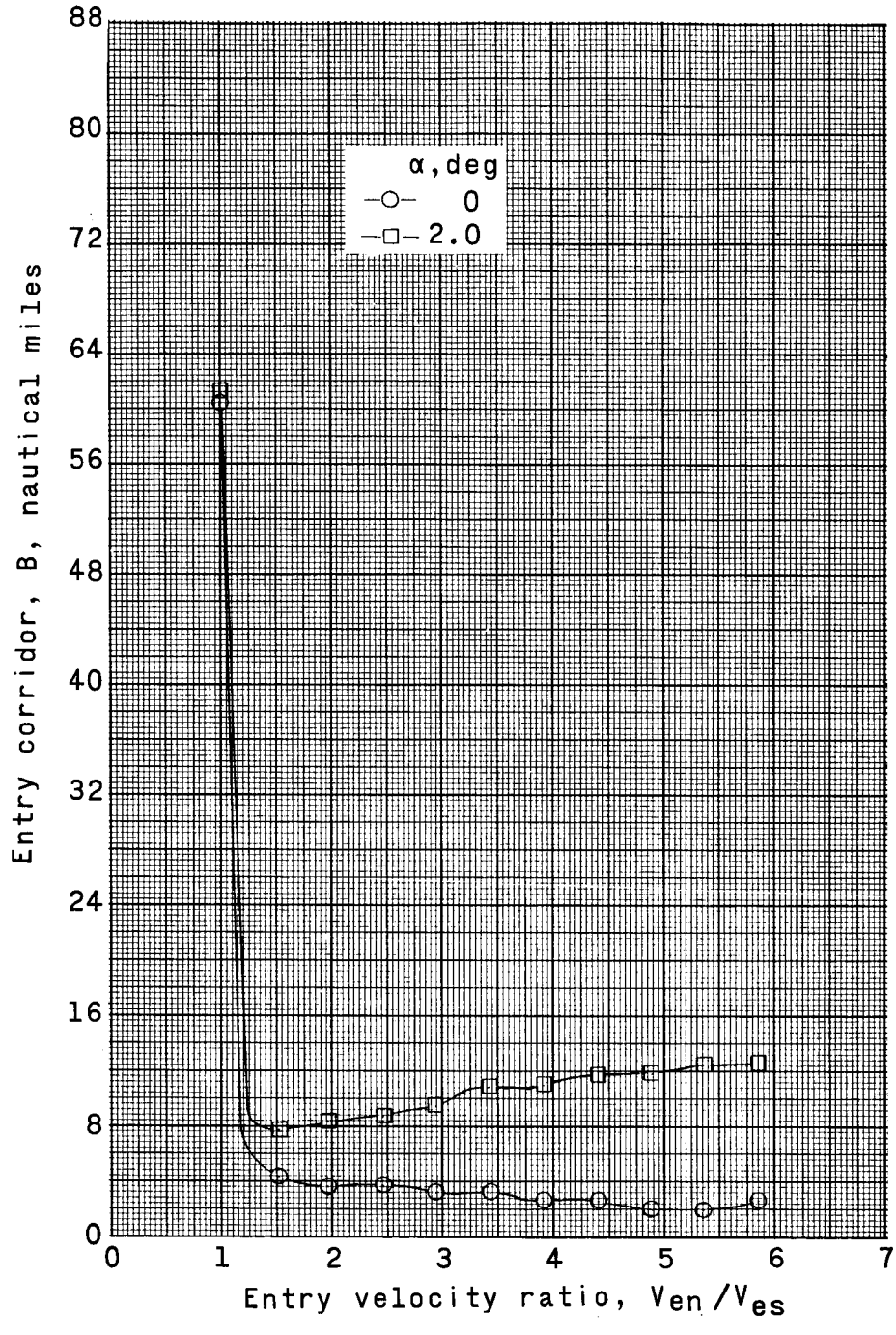

(c) $\frac{W}{C_D A}$ = 29.6 lb/ft^2; C_D = 2.50.

Figure 6.- Continued.

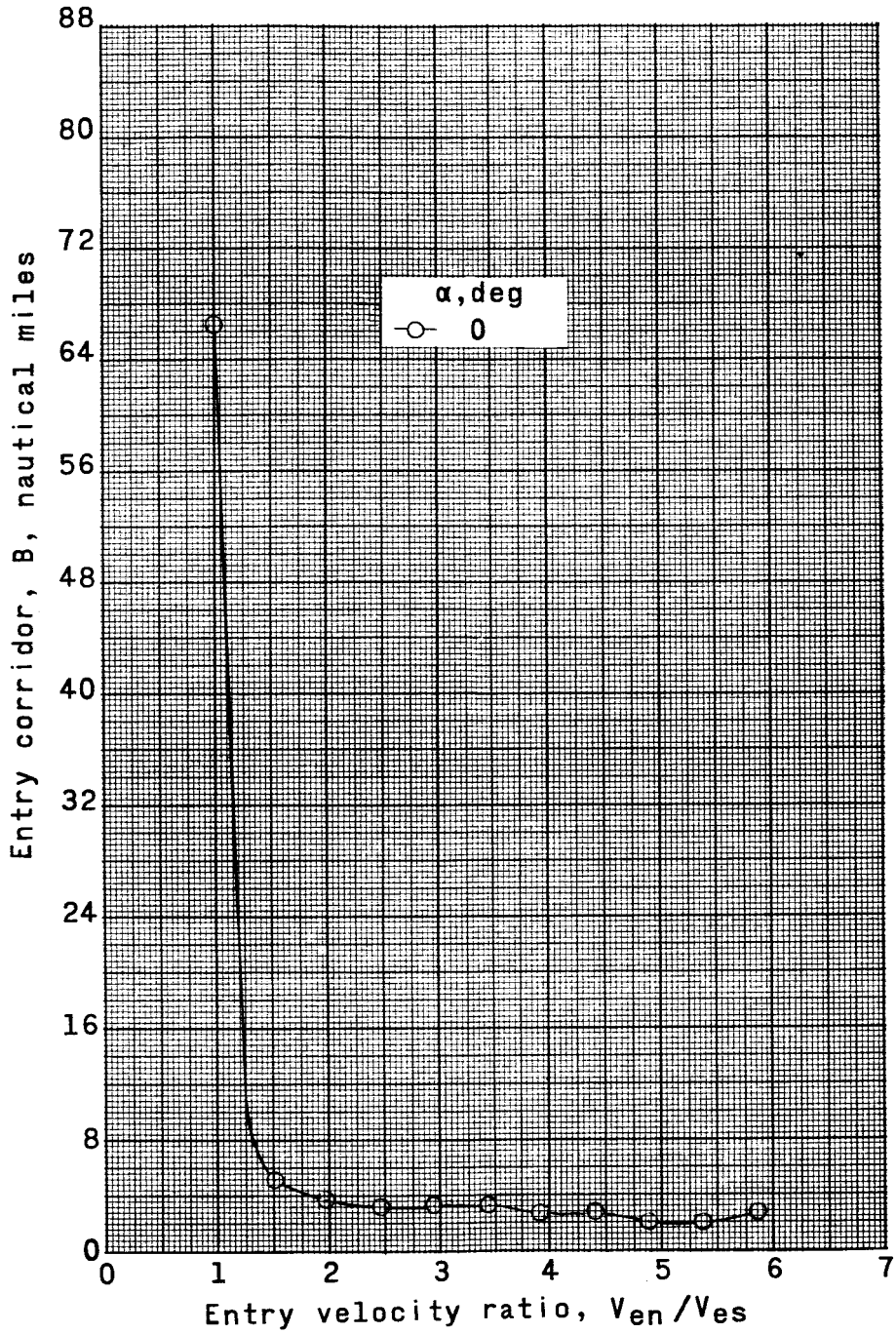

(d) $\frac{W}{C_D A}$ = 71 lb/ft^2; C_D = 1.00.

Figure 6.- Concluded.

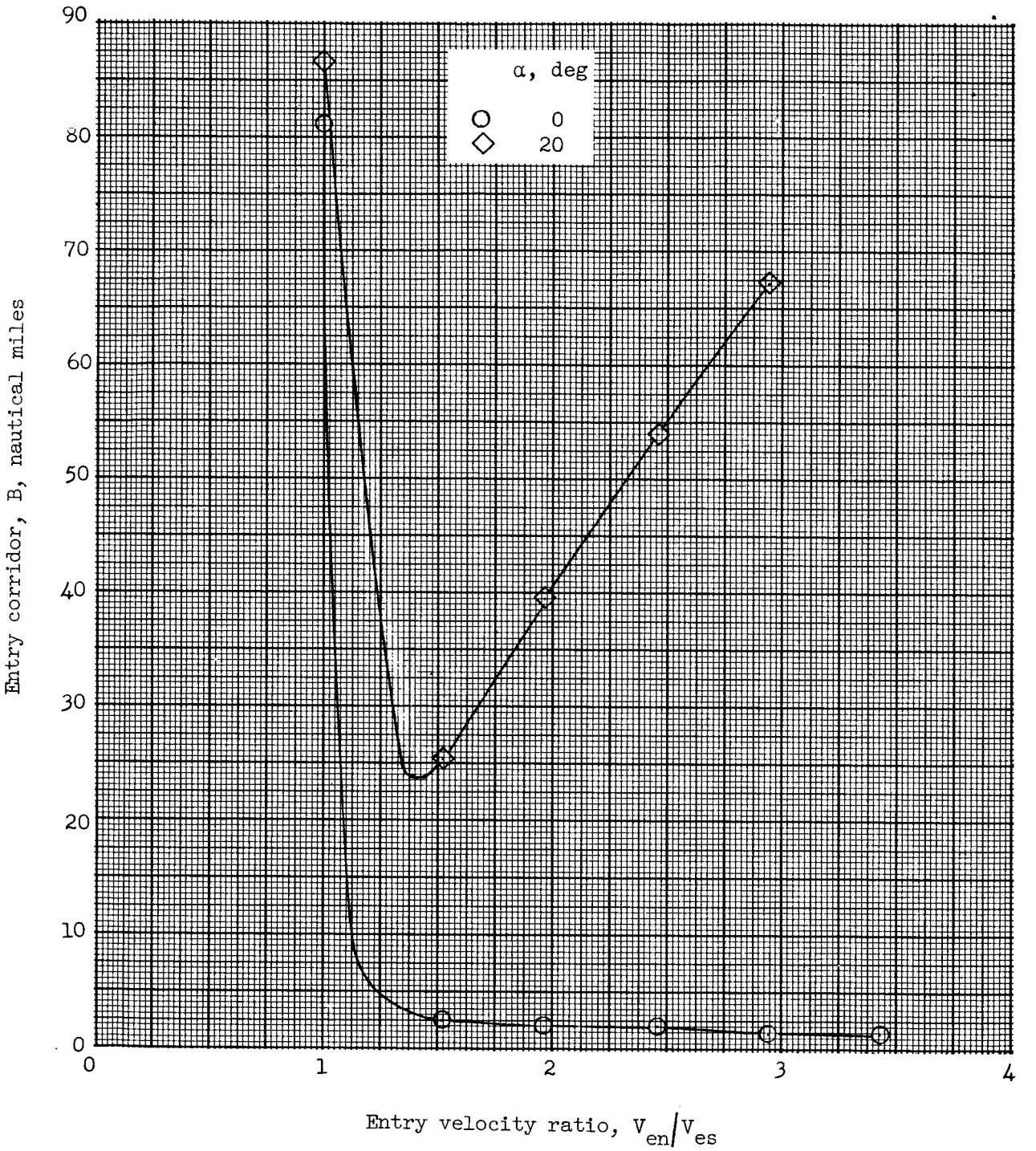

Figure 7.- Entry corridor in nautical miles plotted against entry velocity ratio for the newer less-dense model of the atmosphere. Basic condition; $\frac{W}{C_D A}$ = 51.7 lb/ft^2; C_D = 1.43.

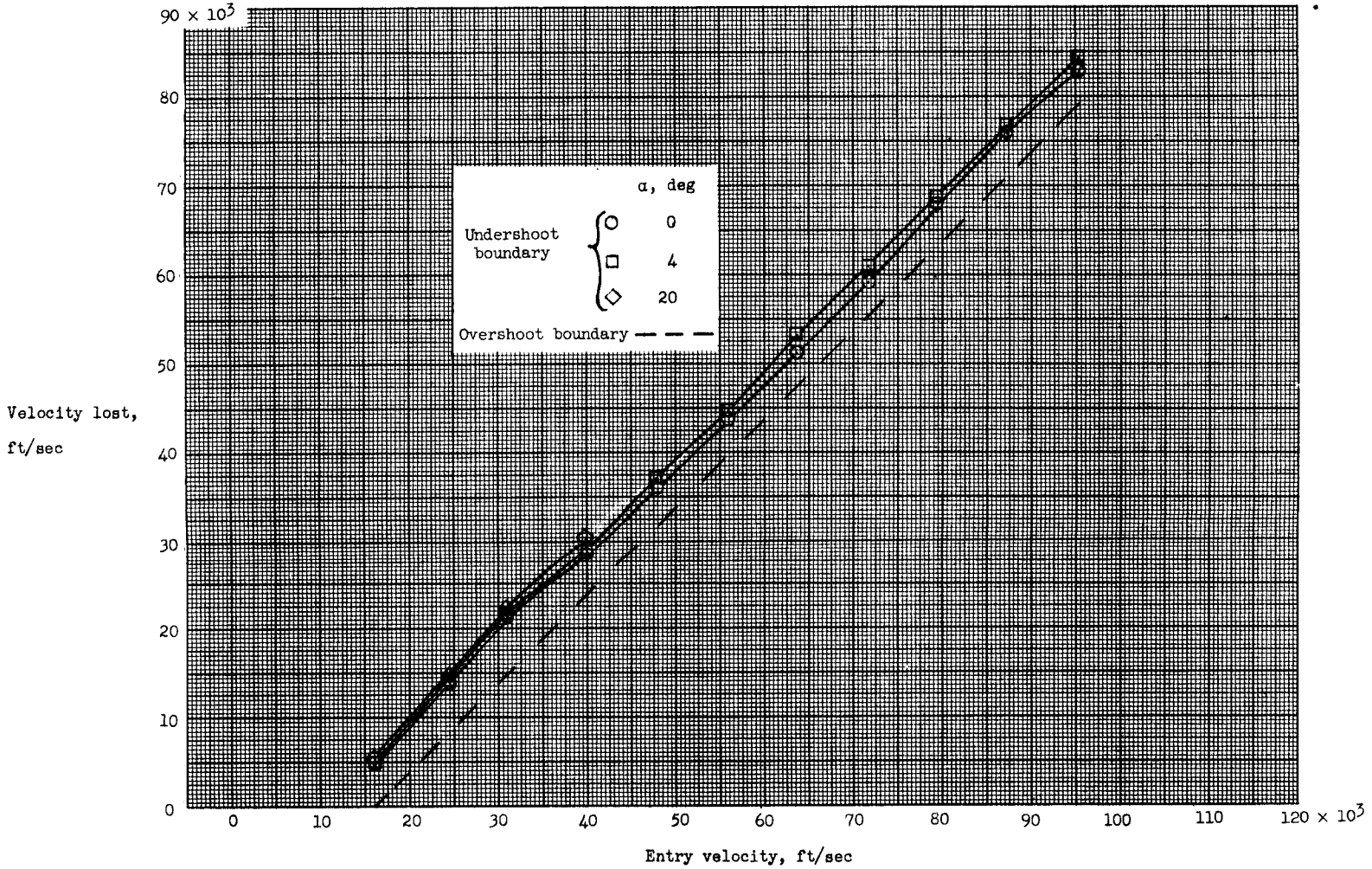

(a) Basic condition; $\frac{W}{C_D A}$ = 51.7 lb/ft^2; C_D = 1.43.

Figure 8.- Velocity lost due to atmospheric braking plotted against entry velocity for the original atmosphere model.

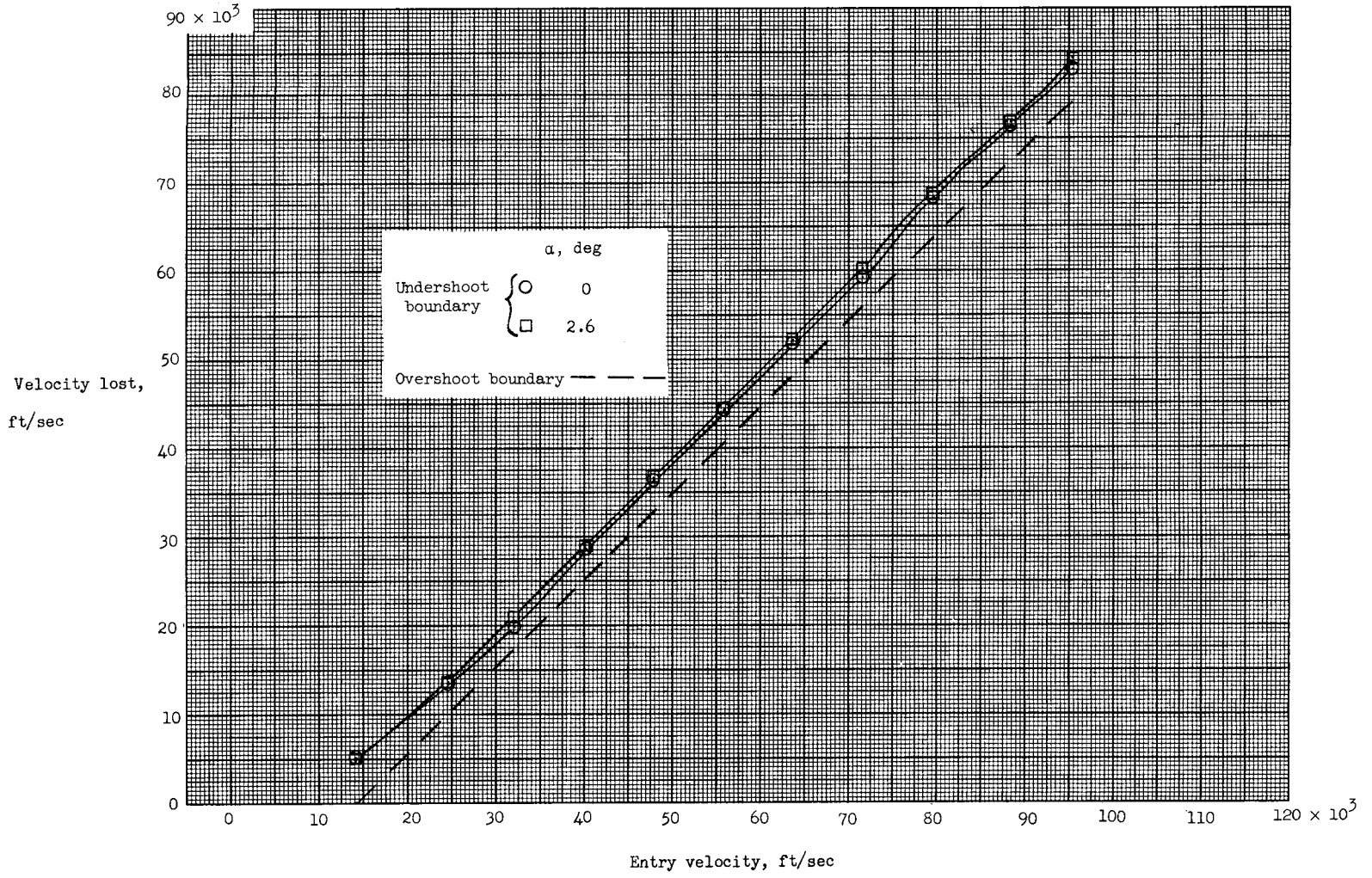

(b) $\frac{W}{C_D A}$ = 37.0 lb/ft^2; C_D = 2.00.

Figure 8.- Continued.

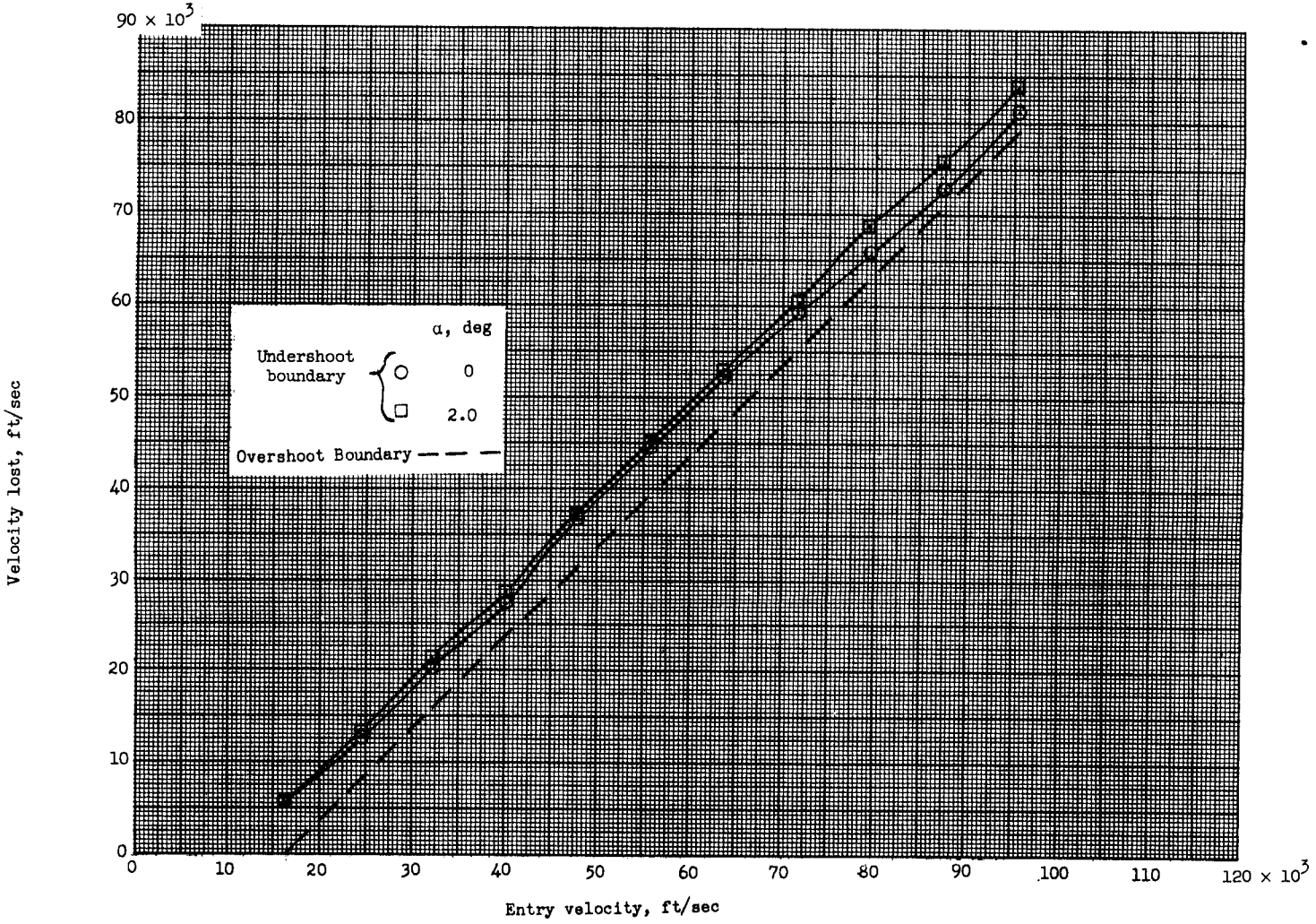

(c) $\frac{W}{C_D A} = 29.6$ lb/ft^2; $C_D = 2.50$.

Figure 8.- Continued.

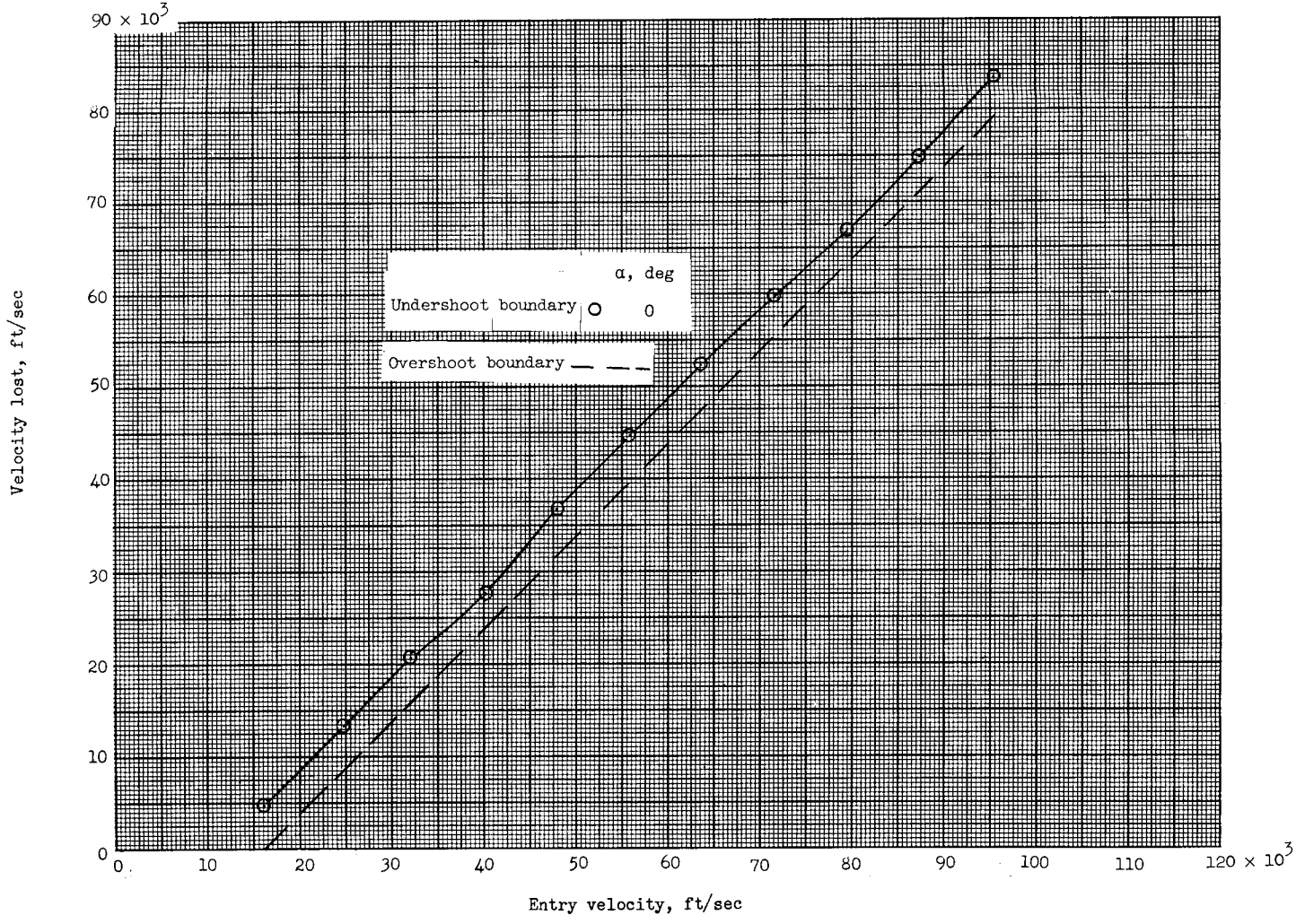

(d) $\frac{W}{C_D A}$ = 74.0 lb/ft^2; C_D = 1.00.

Figure 8.- Concluded.

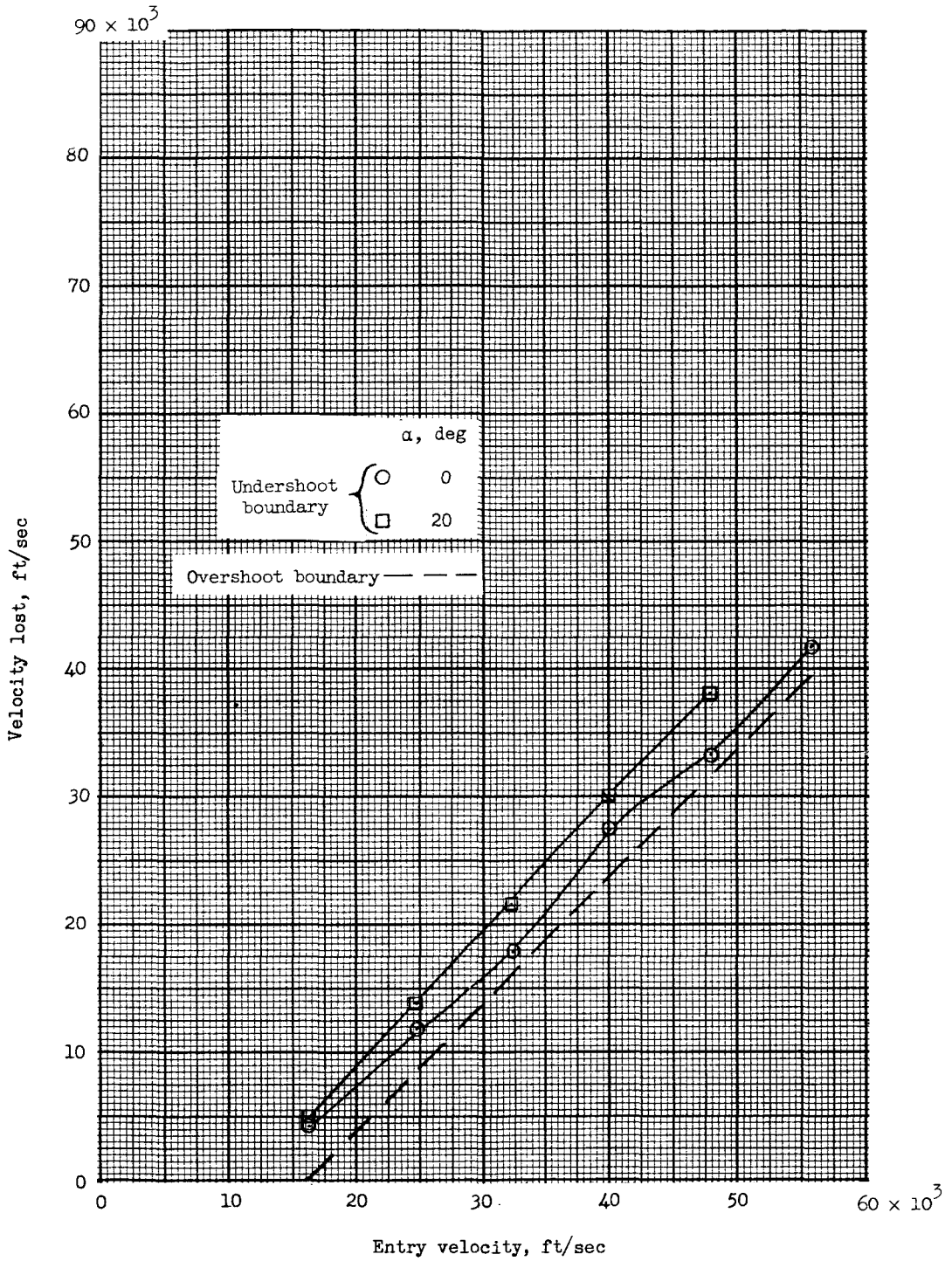

Figure 9.- Velocity lost due to atmospheric braking plotted against entry velocity for the newer less-dense atmosphere model. Basic condition; $\frac{W}{C_D A}$ = 51.7 lb/ft^2; C_D = 1.43.

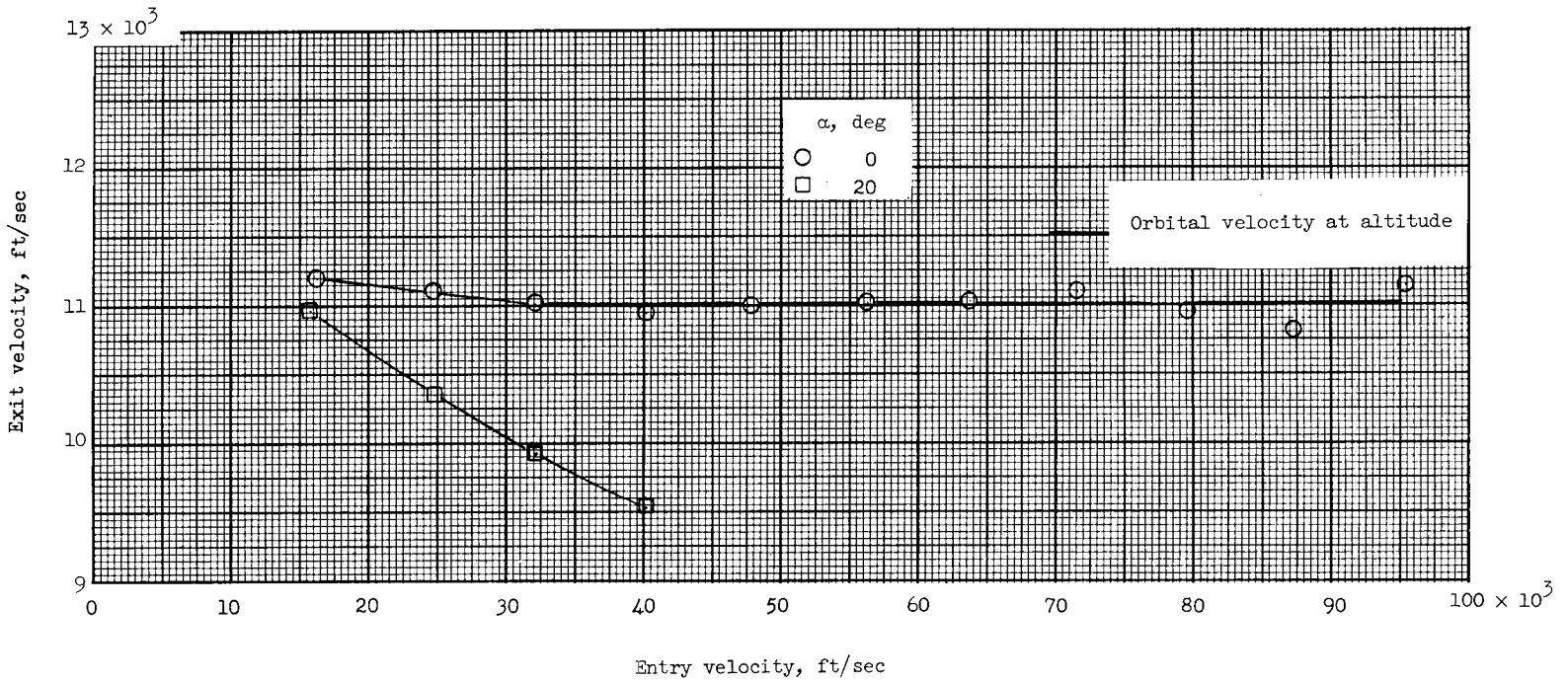

Figure 10.- Velocity at which the vehicle leaves the atmosphere for the undershoot boundary plotted against entry velocity for original atmosphere model. Basic condition; $\frac{W}{C_D A}$ = 51.7 lb/ft^2; C_D = 1.43.

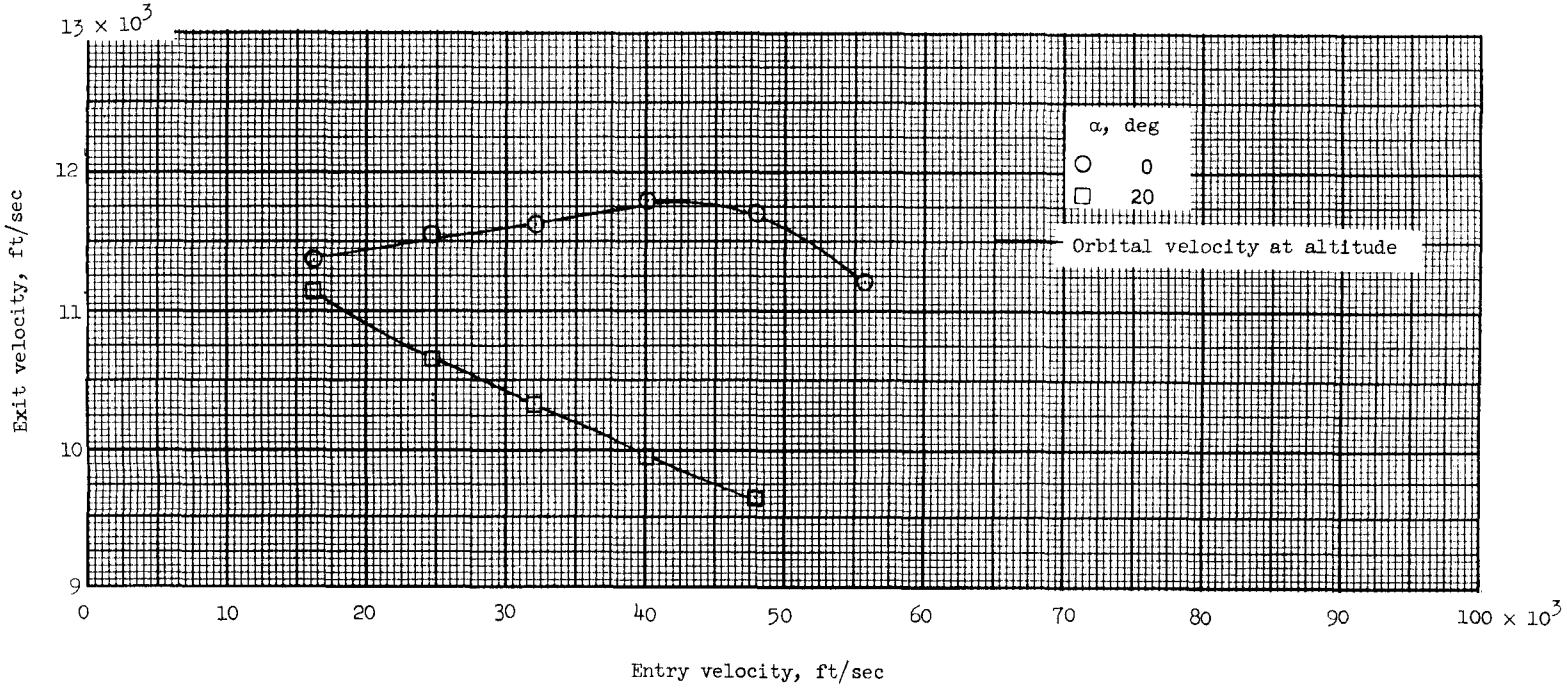

Figure 11.- Velocity at which vehicle leaves atmosphere for undershoot boundary plotted against entry velocity for the newer less-dense atmosphere model. Basic condition; $\frac{W}{C_D A} = 51.7$; $C_D = 1.43$.

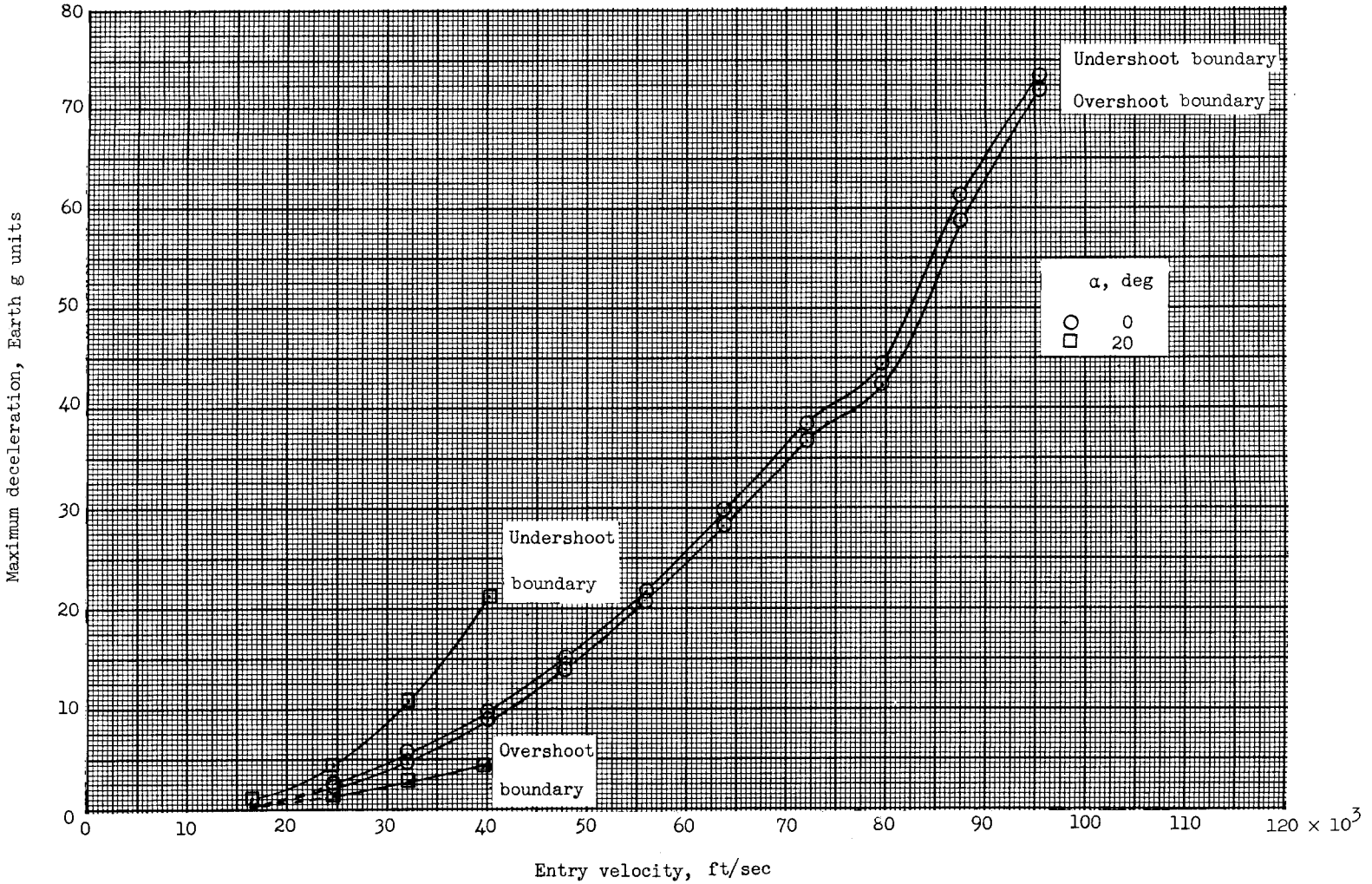

(a) Basic condition; $\frac{W}{C_D A} = 51.7$; $C_D = 1.43$.

Figure 12.- Variation of maximum deceleration with entry velocity for the original model of the atmosphere.

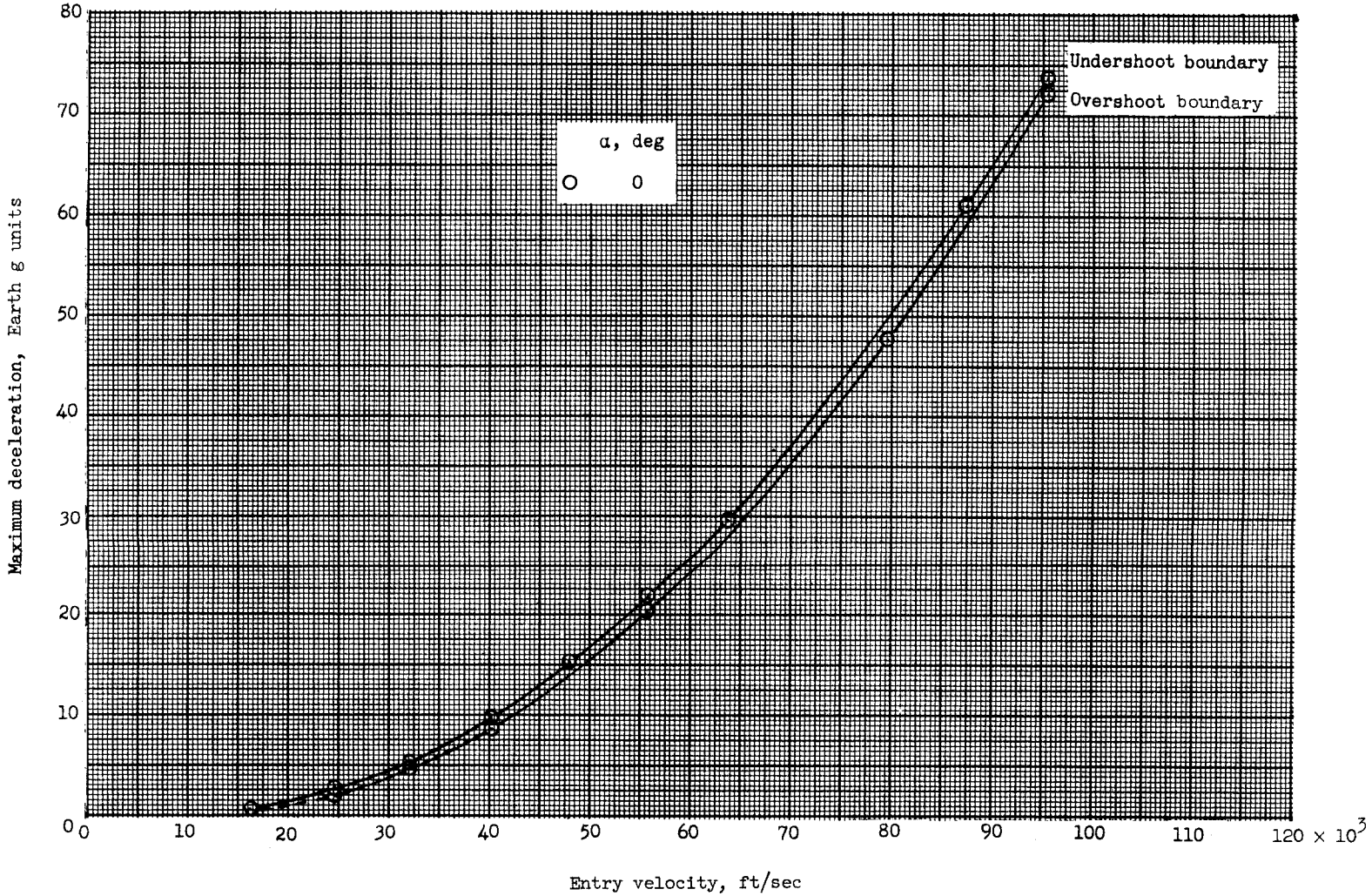

(b) $\frac{W}{C_D A} = 37.0$; $C_D = 2.00$.

Figure 12.- Continued.

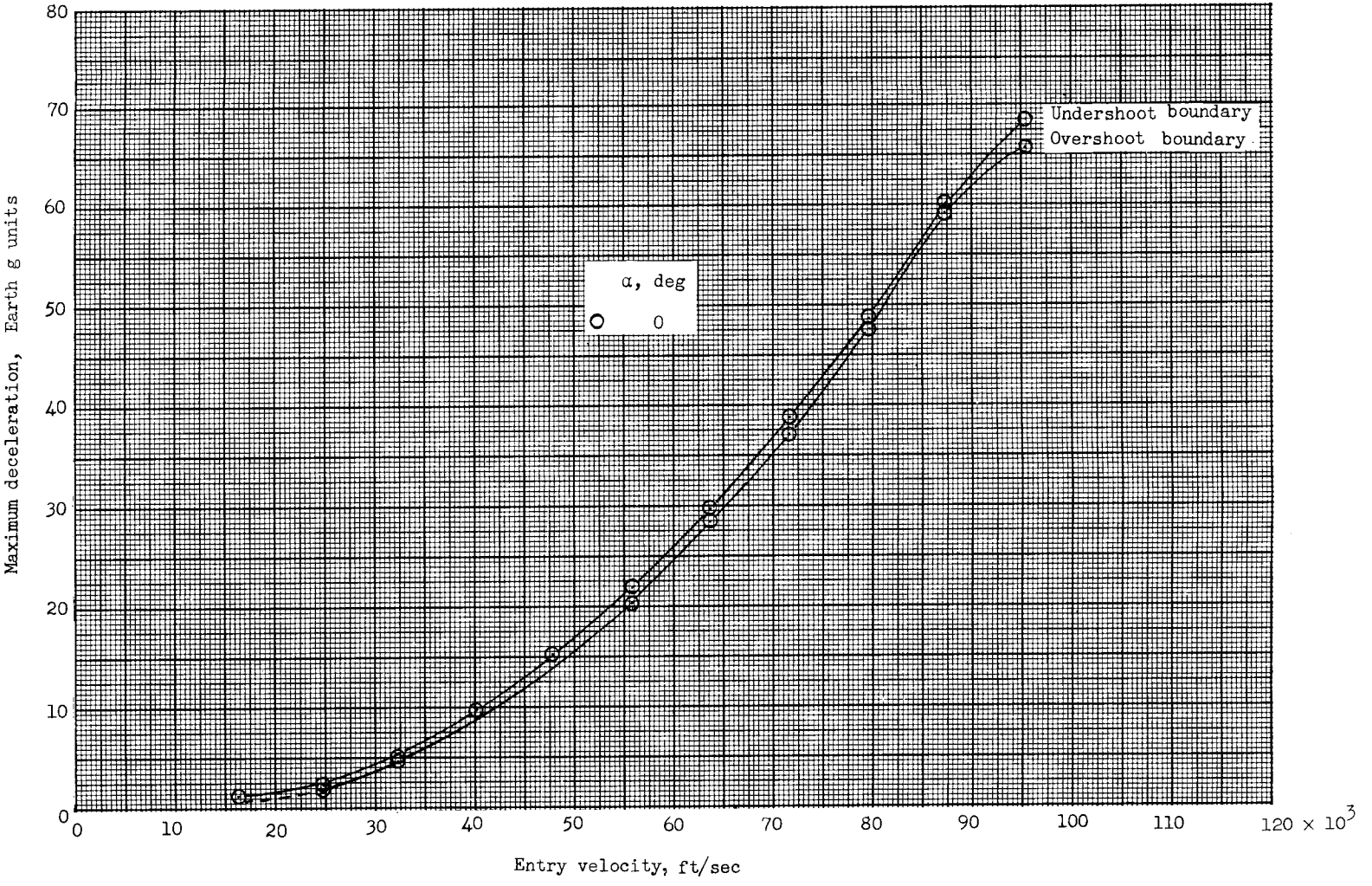

(c) $\frac{W}{C_D A} = 29.6$; $C_D = 2.50$.

Figure 12.- Continued.

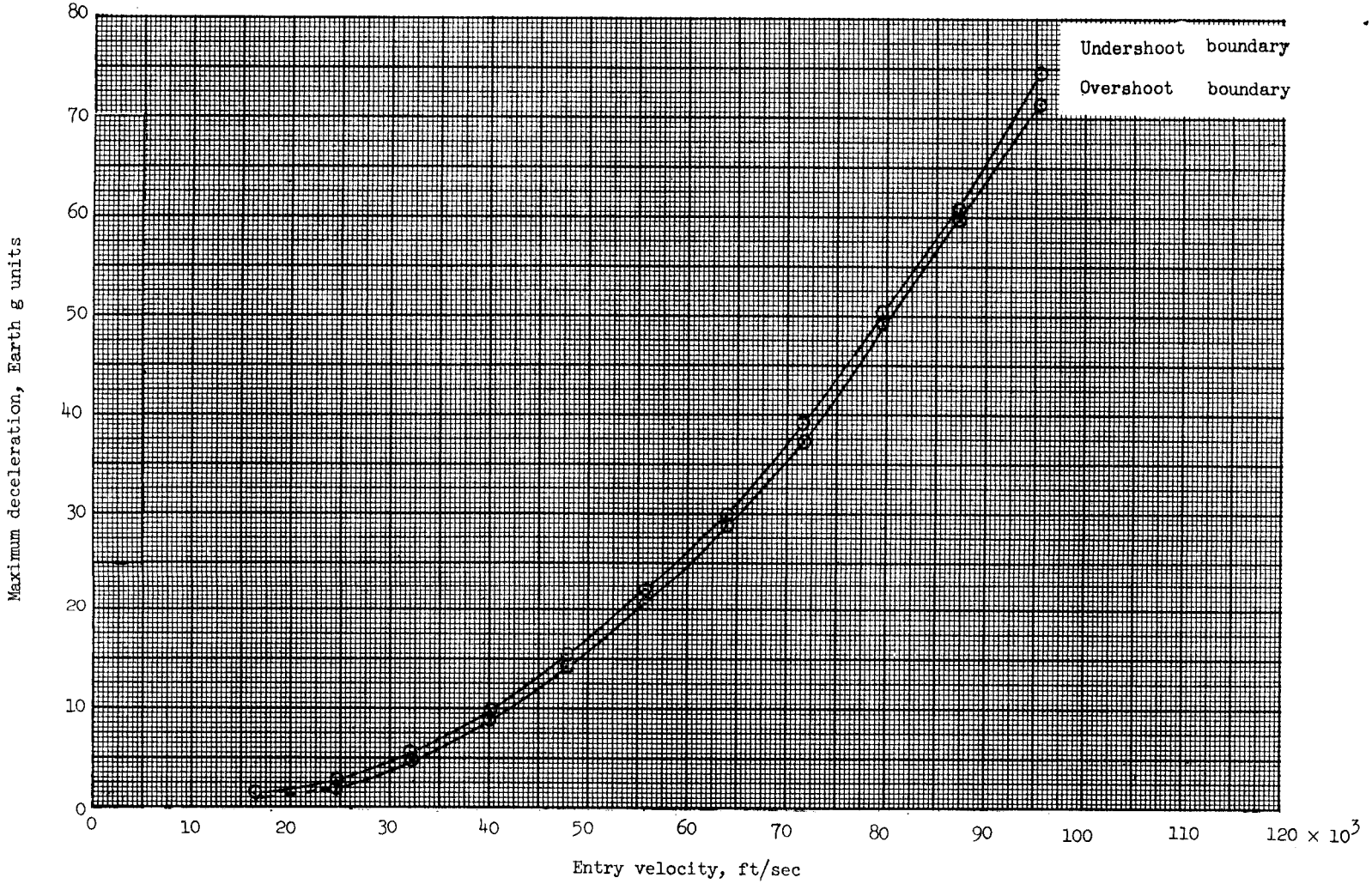

(d) $\frac{W}{C_D A} = 74.0$; $C_D = 1.00$.

Figure 12.- Concluded.

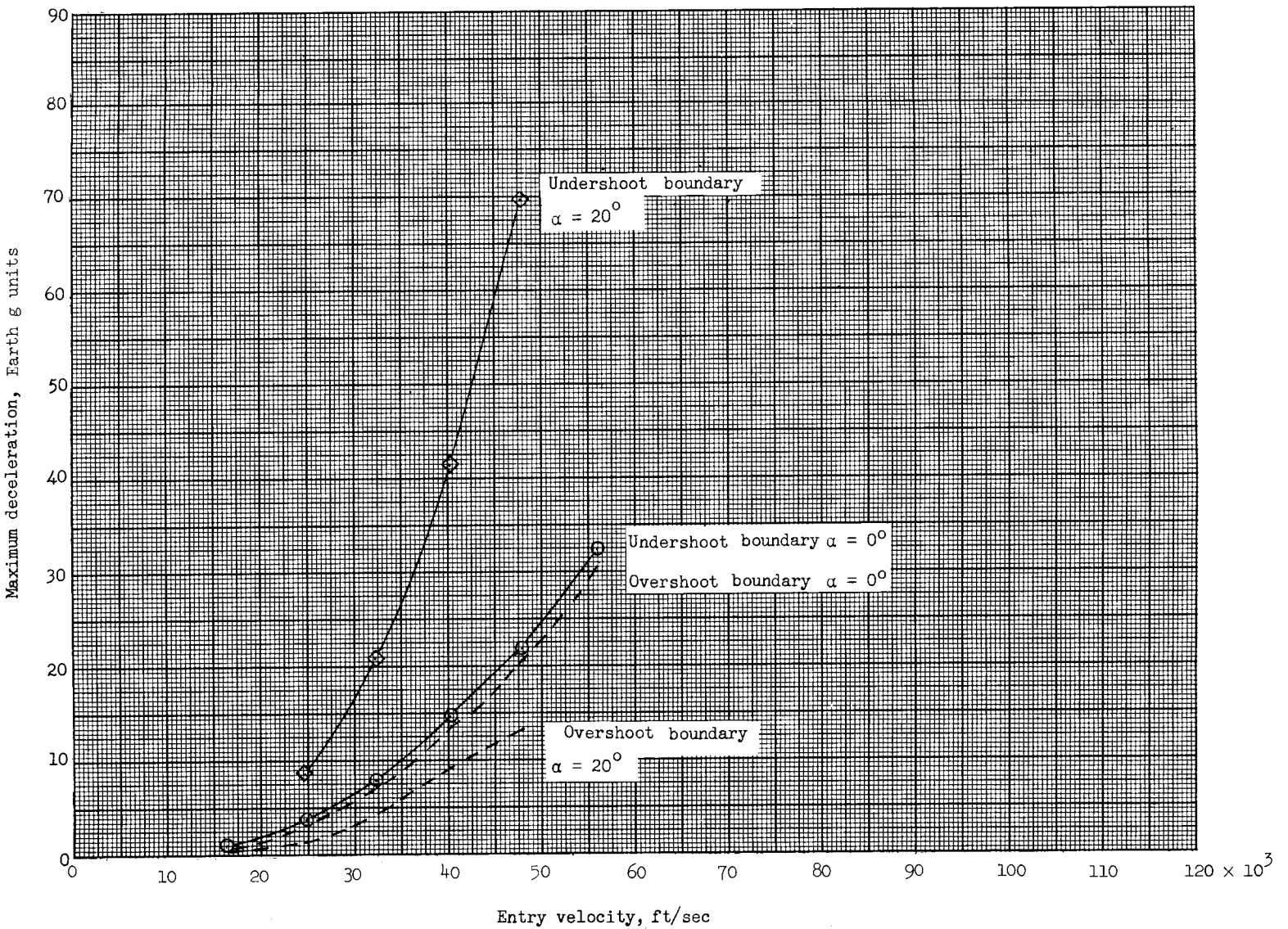

Figure 13.- Variation of maximum deceleration with entry velocity for angles of attack of 0° and 20°. Newer atmosphere model. $\frac{W}{C_D A} = 57.1$; $C_D = 1.43$.

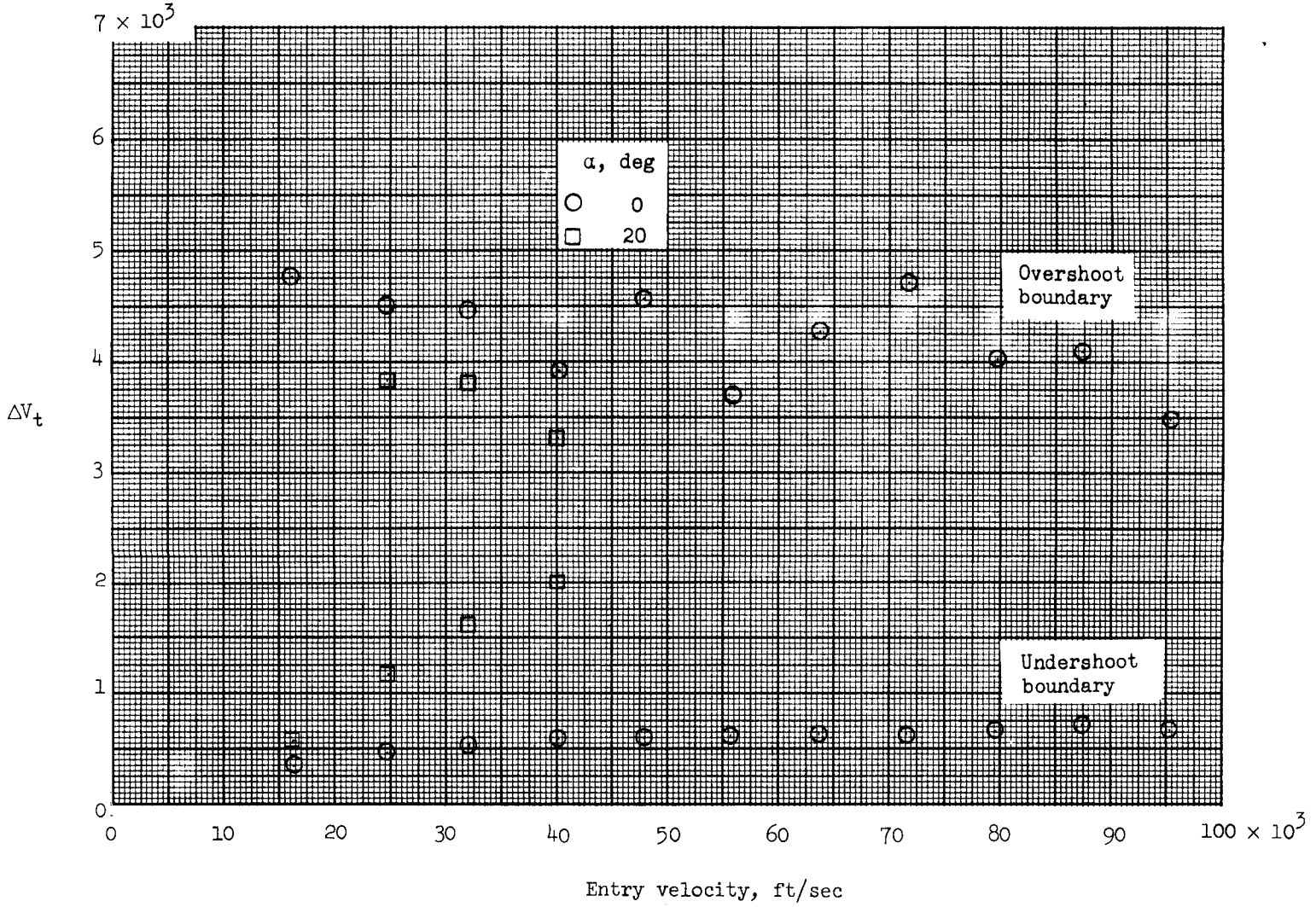

Figure 14.- Variation of the velocity to circularize the orbit after braking with entry velocity. Plotted for the under and overshoot boundaries. Original atmosphere. Basic condition; $\frac{W}{C_D A} = 51.7$; $C_D = 1.43$.

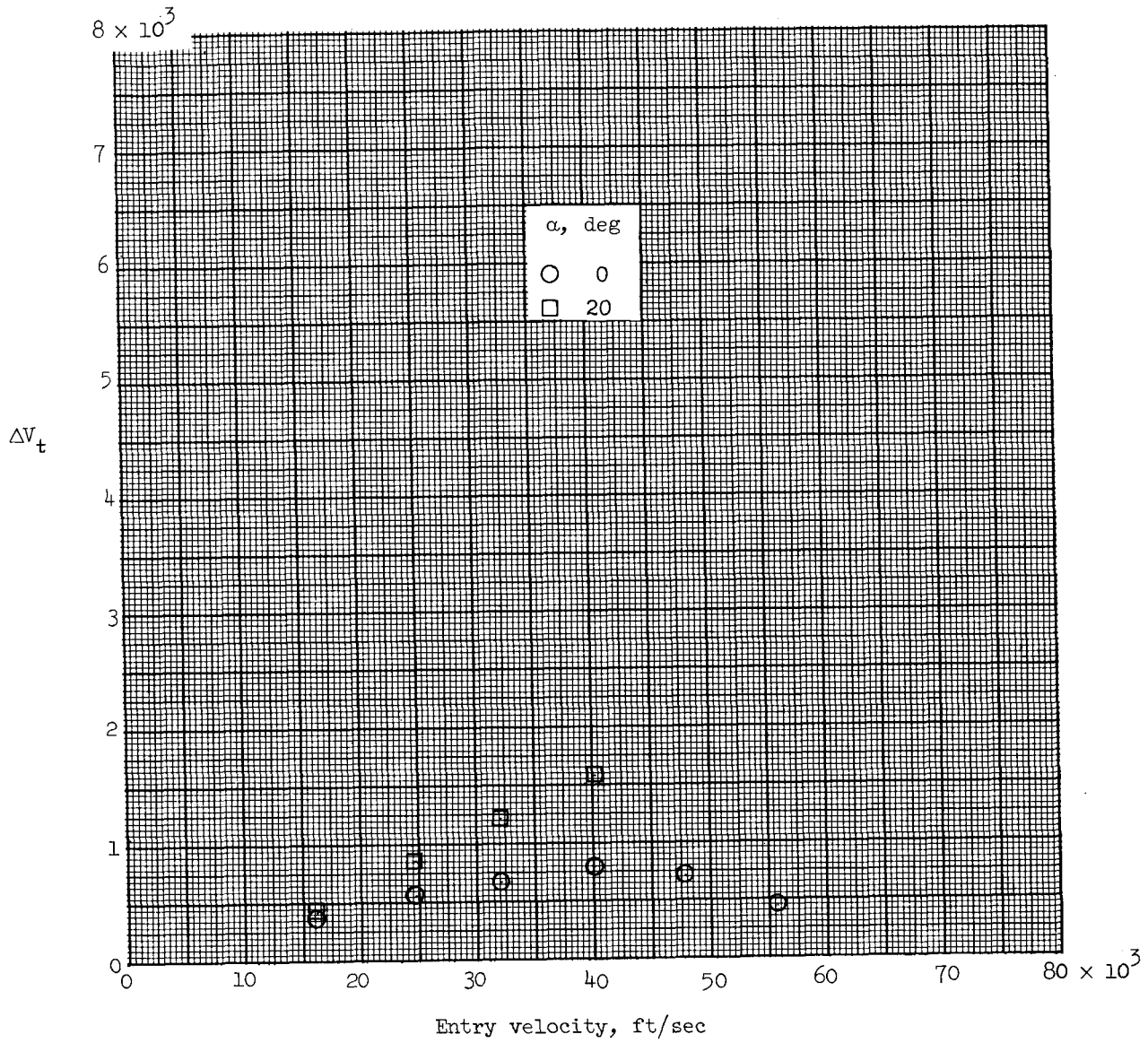

Figure 15.- Variation of the velocity necessary to circularize the orbit after braking with entry velocity. Plotted for the undershoot boundary. Newer atmosphere. $\frac{W}{C_D A} = 51.7$; $C_D = 1.43$.

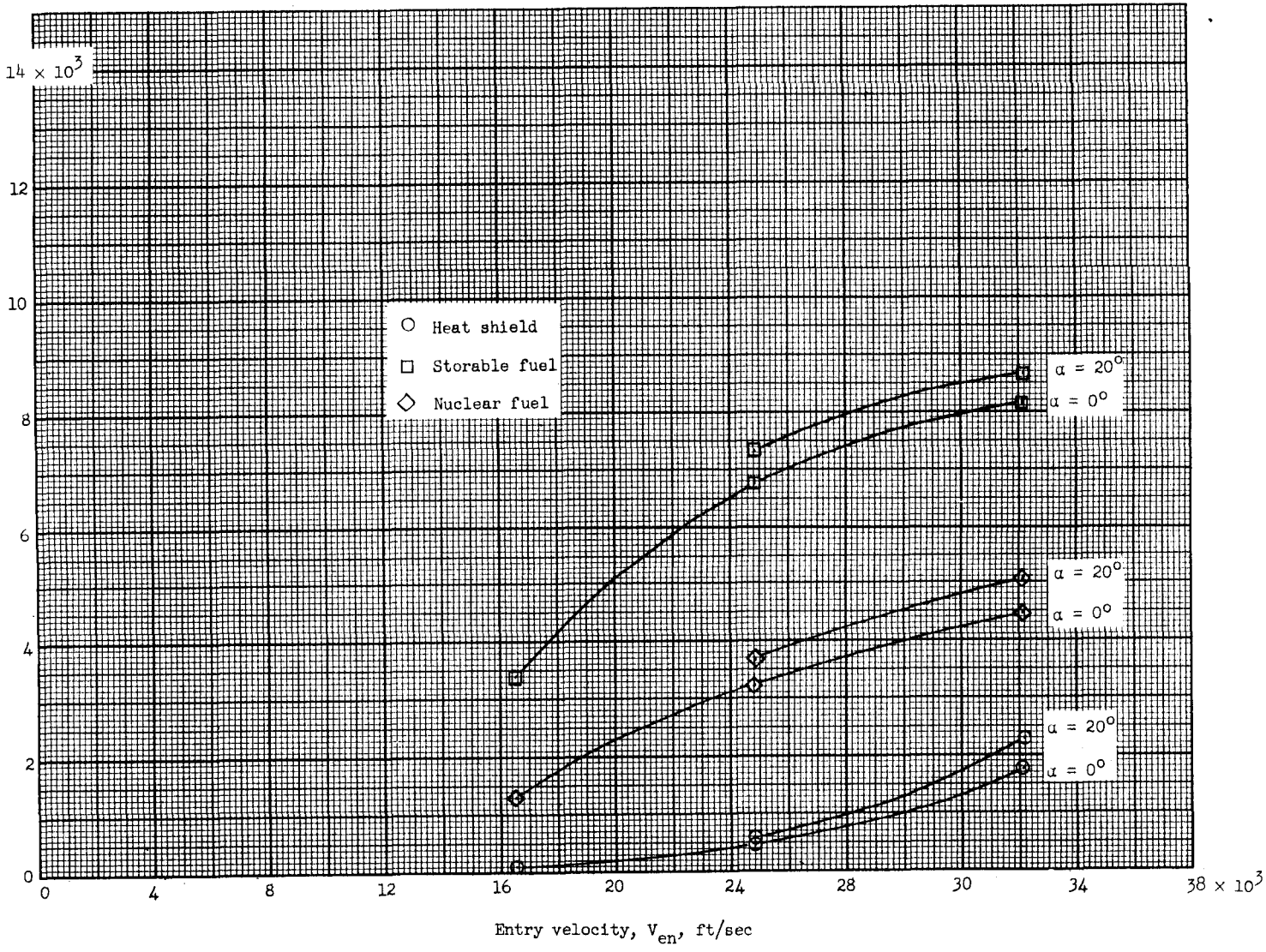

Figure 16.- Weight required for braking by aerodynamic means in newer less-dense atmosphere and by thrust plotted against entry velocity.

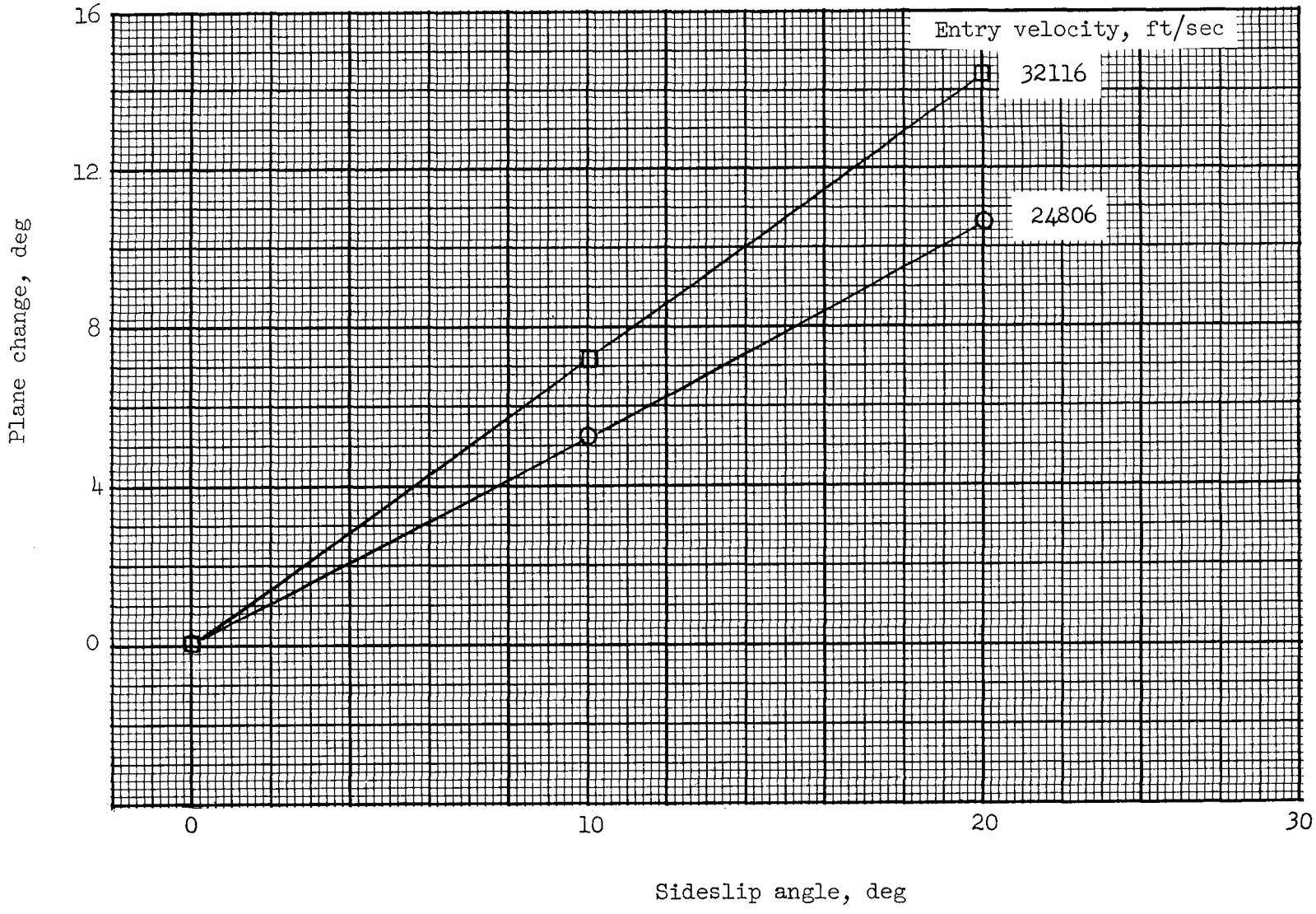

Figure 17.- Amount of plane change possible in original atmosphere for two sideslip angles and two entry vehicles.

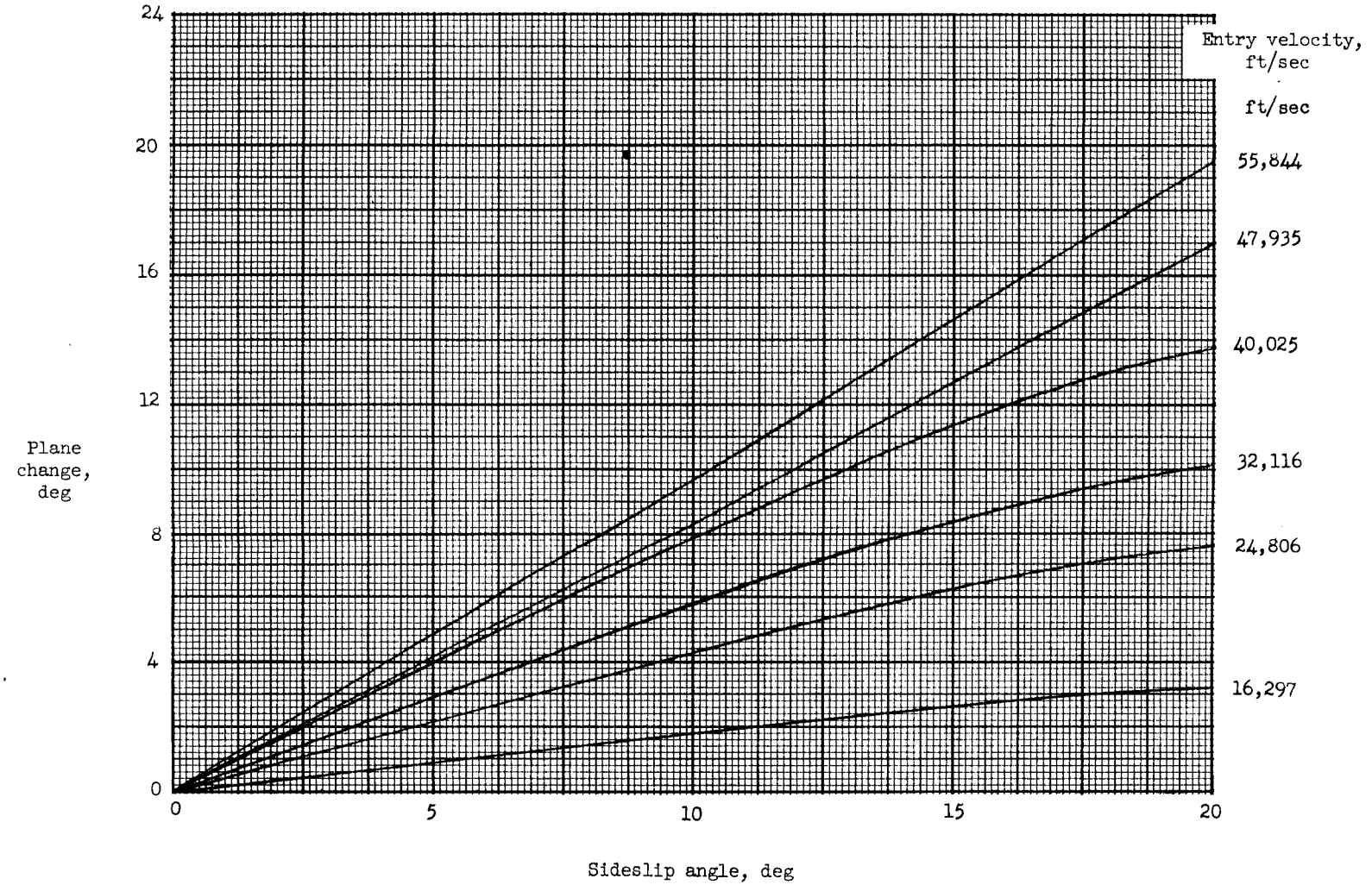

(a) Effect of sideslip angle for various entry velocities.

Figure 18.- Amount of plane change possible in newer less-dense atmosphere for several angles of sideslip and entry velocities.

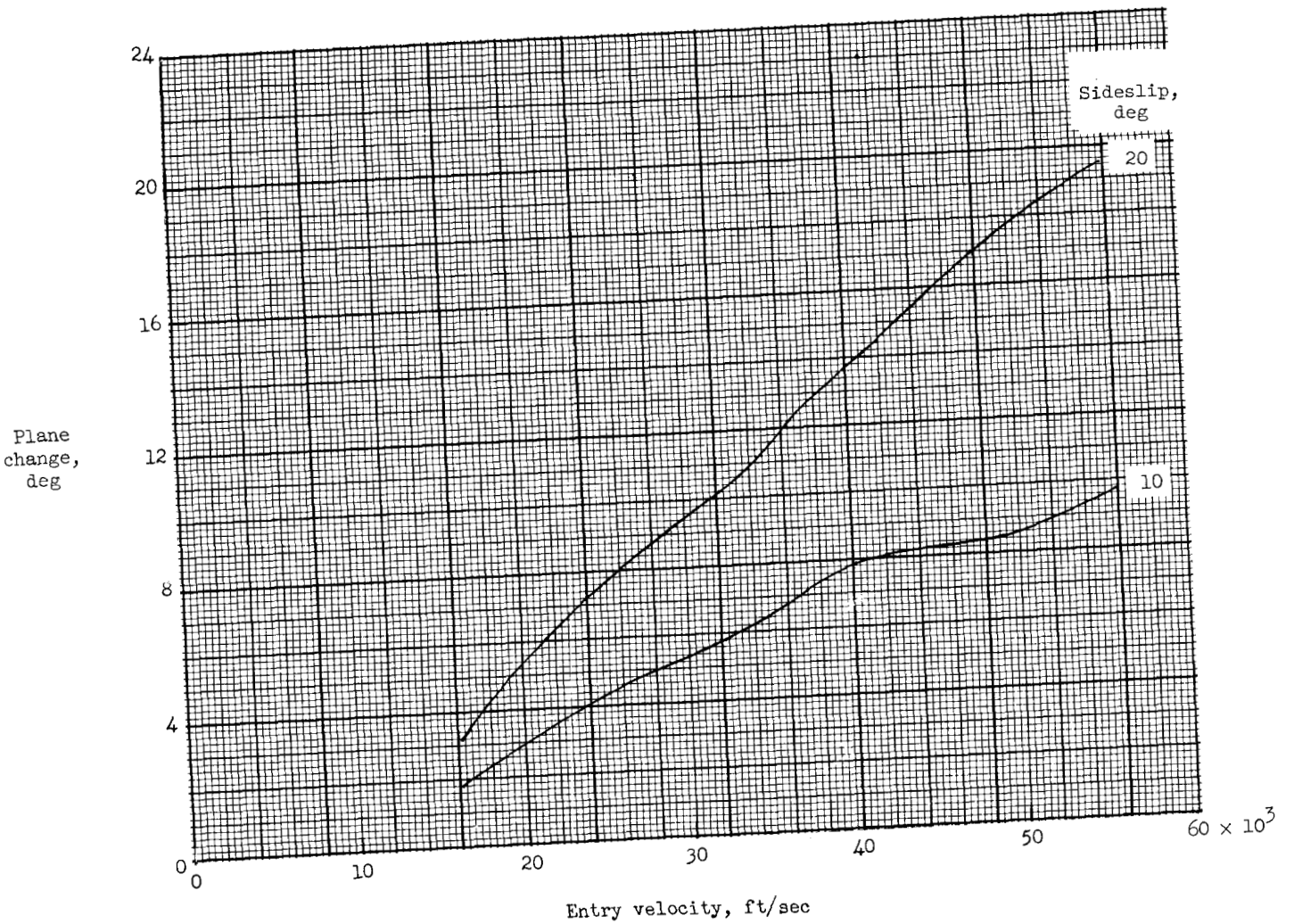

(b) Effect of entry velocity for two sideslip angles.

Figure 18.- Concluded.

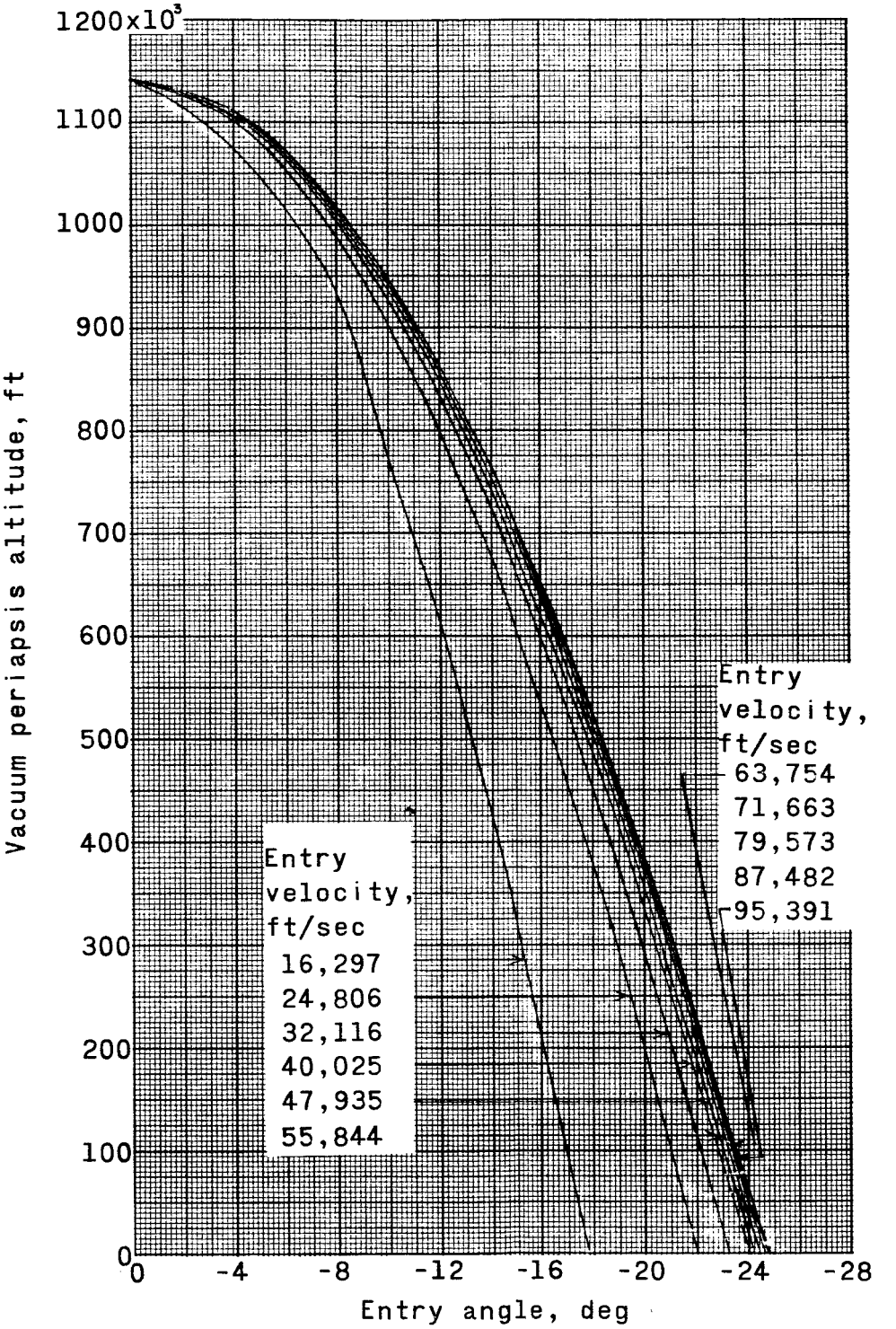

Figure 19.- Vacuum periapsis altitude plotted against entry angle for various approach velocities.